Advances in Nano Research, *Vol. 9, No. 3 (2020) 193-210*
DOI: https://doi.org/10.12989/anr.2020.9.3.193

Several models for bending and buckling behaviors of FG-CNTRCs with piezoelectric layers including size effects

Farshad Heidari[1], Ahmad Afsari[1] and Maziar Janghorban[*2]

[1]*Department of Mechanical Engineering, Shiraz Branch, Islamic Azad University, Shiraz, Iran*
[2]*Department of Mechanical Engineering, Marvdasht Branch, Islamic Azad University, Marvdasht, Iran*

(*Received January 14, 2020, Revised August 12, 2020, Accepted August 14, 2020*)

Abstract. In this research, beside presenting real images of produced Functionally Graded Carbon Nanotube-Reinforced Composites (FG-CNTRCs) and a brief review of the synthesis method of FG-CNTRCs, static and buckling analysis of FG-CNTRC with piezoelectric layers are investigated. It is assumed that the material properties of FG-CNTRC are varied through the thickness direction using four different distributions of Carbon Nanotubes (CNTs). To capture the size effects, nonlocal elasticity theory proposed by A.C. Eringen is also adopted in our model. One of the topics in our paper is using a higher order theory with eight different displacement fields and comparing their results with each other. To solve the governing equations, an analytical method is used to find the deflections and critical buckling loads of FG-CNTRCs. To show the accuracy of present methodology, our results are compared with the results of simply supported rectangular nano plates available in the literature. In this research, the effects of aspect ratio, piezoelectric layer and nonlocal parameter are also studied. It is hoped that this work leads to more accurate models on FG-CNTRC.

Keywords: functionally graded carbon nanotube-reinforced composite; nonlocal elasticity theory; bending; buckling; higher order shear deformation theory; Eight different displacement fields; piezoelectric layer

1. Introduction

In fact, modern achievements in engineering sciences are defined by getting closer to human needs. Nano-technology and nanoscience are attractive research topics that have been taken into considerations in the past decades for this purpose (Kong and Ohadi 2010, Vellingiri *et al*. 2013, Li *et al*. 2013, Amanullah *et al*. 2011, Elkhatib *et al*. 2019, Han *et al*. 2019, Zhang *et al*. 2013, Asmatulu *et al*. 2013, Hanus and Harris 2013, Al-Nemrawi *et al*. 2019). Nowadays, the importance of nanostructures in the development of various industries is well known. In this article, as the first step in reviewing the literature, we present a review on the study of nanobeams, or beam models for nanotubes, then we focus on nanoplates. After that, nanocomposites are investigated. Bedia *et al*. (2019) developed a novel two variable shear deformation beam theory and applied it to investigate the combined effects of nonlocal stress and strain gradient on the bending and buckling behaviors of nanobeams by using the nonlocal strain gradient theory. Equations of motion were obtained via Hamilton's principle. It was seen that the proposed theory was not only accurate and simple in solving the bending and buckling behaviour of nanobeams, but also comparable with the other shear deformation theories which contain more number of unknowns. Matouk *et al*. (2020) investigated the nonlocal integral Timoshenko beam theory for the free vibration analysis of P-FG and symmetric S-FG nanobeams seated on Winkler Pasternak foundation subjected to the thermal and hygrothermal loading. They used the nonlocal theory of Eringen to capture the size effect and studied the effects of the various parameters influencing the vibrational responses of the P-FG and SS-FG nanobeams. Reddy (2007) corrected local beam theory by using the nonlocal differential fundamental relations of Eringen to study bending, vibration, and buckling behaviors of nanobeams. It was seen that the inclusion of the nonlocal effect increases the magnitudes of deflections and decreases buckling loads and natural frequencies. Pradhan and Murmu (2010) developed a single nonlocal beam model to study the static and vibration specification of a nanocantilever beam. It was shown that the small-scale effect on the frequency response was increased for first mode of vibration while it was decreased for higher modes of vibration. Demir *et al*. (2010) proposed discrete singular convolution procedure to study free vibration of carbon nanotubes modeled by Timoshenko beam. Lu *et al*. (2017) researched static bending and buckling behaviors of nanobeams based on an integrated size-dependent high-order beam model who contains different higher order shear deformation beam models as well as Euler-Bernoulli and Timoshenko beam models and the nonlocal strain gradient theory. It was shown that the nanobeam could exhibit either stiffness-softening effect or stiffness-hardening effect, which depends on the relative magnitude of the nonlocal parameter and the material length scale parameter. Peddieson *et al*. (2003) used the nonlocal continuum theory

*Corresponding author, Ph.D.,
E-mail: maziar.janghorban@miau.ac.ir,
maziar.janghorban@gmail.com

ISSN: 2287-237X (Print), 2287-2388 (Online)

to develop the nonlocal Euler-Bernoulli beam model for the static analysis of beam. They concluded that the nonlocal effect could be beneficial and considerable for nanostructures. In their work, the nonlocal effect was disappearing for a cantilever beam subjected to any mixture of concentrated loads.

Nanoplate is a typical structure of nanoscale systems, which can be deformed into the nanotube and made as the MEMS/NEMS component. Li (2014) used the variation method to extract the governing equations to determine the buckling behavior of the magnetoelectroelastic (MEE) nanoplate based on the Mindlin theory. These results may be useful in the analysis and design of smart structures constructed from magnetoelectroelastic materials. Balubaid *et al*. (2019) investigated the free vibrational behavior of simply supported FG nanoplate by using the nonlocal two variables integral refined plate theory. The equations of motion of the system were determined and resolved via Hamilton's principle and Navier method, respectively. Farajpour *et al.* (2016) studied size dependent free vibrations of MEE nanoplate using a nonlocal continuum elastic model. In this research, the nanoplate was supposed to be under magnetic and electric potentials. The governing equations and boundary conditions were extracted using the Hamilton principle and the use of nonlocal elasticity theory. Arani *et al*. (2016) investigated the linear free vibration of rectangular nanoplate created of magnetostrictive materials. Considering orthotropy angle, they concentrated on the elastic medium as an efficient stability factor. Nami and Janghorban (2015a) studied dynamic analysis of rectangular nanoplates subjected to moving load with constant velocity. In order to derive the governing equations of motion, second order plate theory was used. To solve the governing equations, state-space method was used to find the deflections of rectangular nanoplate under moving load. The obtained results revealed that the nonlocality has significant effect on the deflection of rectangular nanoplate subjected to moving load. The dynamics of the interaction between a Kirchhoff nanoplate and the surrounding fluid was investigated by Hosseini *et al*. (2019). Using nonlocal elasticity theory, the influence of small-scale parameter was considered in the governing equation of motion. The vibration behavior of nanoplate submerged in different viscous fluids with various aspect ratios were simulated in order to analyze the effects of fluid viscosity and density on the free vibration natural frequencies of the nanoplate. The results shown that, for smaller size parameter, the fluid existence has a remarkable decreasing effect on the nanoplate natural frequencies. Nami and Janghorban (2015b) studied the free vibration of simply supported rectangular nanoplates based on two-variable refined plate theory using strain gradient elasticity theory. Strain gradient elasticity theory with two gradient constants was used. Karami *et al*. (2019a) investigated buckling behavior of functionally graded nanoplates made of anisotropic material (beryllium crystal as a hexagonal material) including the influences of different boundary conditions, small-scale parameters, geometry parameters and exponential factor in detail. Karami *et al*. (2019b) studied the resonance behavior of Kirchhoff nanoplates. To capture the small-scale effects on the resonance deflections of nanoplates, the bi-Helmholtz nonlocal strain gradient theory incorporating three small-scale parameters was adopted. The effects of some parameters such as constant material parameters, aspect ratio and small-scale parameters were investigated in detail. A nonlocal second-order shear deformation formulation was also presented by Karami *et al*. (2019c) to study the size-dependent thermal buckling of embedded sandwich piezoelectric nanoplates with functionally graded core. Based on the developed nonlocal second-order shear deformation theory, the size-dependent equations of motion were derived. The nonlocal thermal buckling responses of simply supported nanoplates were solved via Navier method. The influences of nonlocal parameter, gradient index, electric voltage, and Winkler-Pasternak parameters on the thermal buckling characteristics of functionally graded nanoplates were examined, too.

In general, nanocomposites have been shown to be able to exhibit excellent mechanical, thermal, electrical, and physical properties. Besides, since the discovery in 1991, carbon nanotubes are widely used as the reinforcing nanofillers to develop high-strength nanocomposites owing to their exceptional mechanical properties and chemical stability (Shariati *et al*. 2020, Zhu *et al*. 2012a, Kim *et al*. 2009, Balubaid *et al.* 2019, Li *et al.* 2007, Esawi *et al*. 2010, Moghadam *et al*. 2015). On the other hand, a new type of material is Functional Graded Material (FGM) which is a type of finite composite material that its properties changes from one surface to another with smooth and continuous variations. These functional gradients have advantages such as eliminating material discontinuities and avoiding delamination, reducing pressure levels and flexural deformation (Chikr *et al.* 2020, Rad 2018, Karami *et al*. 2019d, Refrafi *et al*. 2020, Karami and Janghorban 2019, Li *et al.* 2015, Li and Hu 2017, Nami and Janghorban 2014a, She *et al*. 2019). Srividhya *et al*. (2018a) investigated the effect of the material homogenization scheme on the flexural response of a thin to moderately thick FGM plate by using the first-order shear deformation theory. Also, they examined a parametric study bringing out the effect of boundary conditions, loads and power-law index. Khiloun *et al*. (2020) presented a new quasi-3D hyperbolic shear deformation theory for bending and free vibration of FG plates and used the Hamilton's principle to derive the equations of motion. In 2009, a new type of materials has been introduced, called functionally graded carbon nanotube-reinforced composite, which is combined the idea of FGMs and nanocomposites. A study on Functionally Graded Carbon Nanotube-Reinforced Composite (FG-CNTRC) structures has been conducted intensively in the recent years, in vibration, static, dynamic, buckling and post-buckling analyses. Here, we present a brief review on micro-nanocomposites and FG nano-composites. Alimirzaei *et al*. (2019) researched the nonlinear bending, buckling and vibration analysis of viscoelastic micro-composite beam reinforced by various distributions of BNNT with initial geometrical imperfection on elastic foundation. They considered the various distributions of BNNT as UD, FG-V and FG-X and also, used the extended rule of mixture to estimate the properties

of micro-composite beam. Finally, the governing equations of motion for micro-composite beam were obtained using energy method and Hamilton's principle. She *et al*. (2019) studied the novel carbon nanotubes reinforced nano-composite coatings through two-step strategy using both Physical Vapour Deposition (PVD) approach and Chemical Vapour Deposition (CVD) approach. The results indicated that well-composited DLC-CNT nanocomposite coating can be achieved which exhibited better electrical conductivity compare to that of the pristine DLC coating. Amraei *et al*. (2019) presented a closed-form micro-mechanical interphase model considering the diameter of nanotube, the thickness of interphase, and mechanical properties of nanotube and polymer to estimate the overall mechanical properties of nanotube-reinforced polymer nanocomposites. The constituent material of the structure was made of an epoxy matrix which was reinforced by both macro- and nano-size reinforcements, namely Carbon Fiber (CF) and carbon nanotube was studied by Ebrahimi and Dabbagh (2019). Then, on the basis of an energy-based Hamiltonian approach, the equations of motion were derived using the classical theory of plates. Numerical results shown that plates fabricated from the hybrid nanocomposites can endure higher frequencies compared with those consisted of conventional composites. The effect of loading frequency on the dynamic behavior of nanocomposite sandwich plates under periodic thermo-mechanical loadings had been investigated by Safaei *et al.* (2019). The utilized sandwich plates were made of an isotropic polymer material and two symmetric face sheets reinforced by functionally graded distributions of the carbon nanotube agglomerations. Karami *et al*. (2019e) investigated the size-dependent buckling response of FG-CNTRC curved beams based on a higher-order shear deformation beam theory in conjunction with the Eringen's Nonlocal Differential Model (ENDM). Arefi *et al*. (2019) studied a large parametric on the bending response of the functionally graded polymer composite curved beams reinforced by graphene nanoplatelets resting on a Pasternak foundation. The theoretical framework was based on the first order shear deformation theory and the nonlocal elasticity theory. The numerical results were presented in terms of some significant parameters, such as the weight fraction and geometrical features of the graphene nanoplatelets, the total number of layers, the foundation properties and the nonlocal parameter. Duc *et al.* (2019) introduced analytical solutions for the nonlinear vibration of imperfect functionally graded nanocomposite double curved shallow shells on elastic foundations subjected to mechanical load in thermal environments. The influences of geometrical parameters, elastic foundations, initial imperfection, temperature increment, mechanical loads and nanotube volume fraction on the nonlinear thermal vibration of the nanocomposite double curved shallow shells were discussed in numerical results. Wu *et al.* (2019) formulated, based upon the nonlocal strain gradient theory of elasticity, an inhomogeneous size-dependent beam model within the framework of a refined hyperbolic shear deformation beam theory. Thereafter, via the constructed nonlocal strain gradient refined beam model, the nonlinear primary resonance of laminated Functionally Graded Graphene Platelet-Reinforced Composite (FG-GPLRC) microbeams under external harmonic excitation was studied in the presence of the both hardening-stiffness and softening-stiffness size effects. It was found that the nonlocality size effect leads to an increase in the peak of the jump phenomenon and the associated excitation frequency, while the strain gradient size dependency results in a reduction in both of them.

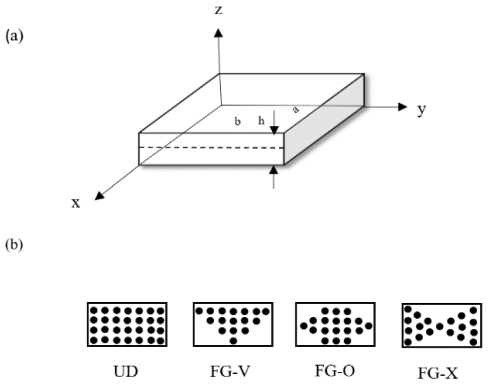

Fig. 1 Functionally graded carbon nanotube-reinforced composite plates

In present article, based upon the nonlocal theory of elasticity, FG-CNTRC within the framework of a higher order shear deformation plate theory with eight different displacement fields is investigated. This FG sandwich nanocomposite has a FG core with nanotubes as reinforcements and two piezoelectric layers at the top and bottom. Deflections and buckling loads are extracted from governing equations of motion using Navier method. It is mentioned that one of the objective of this article is using a higher order theory with eight different displacement fields and comparing their results with each other. Also, in this research, the influences of aspect ratio, piezoelectric layer and nonlocal parameter on the results are presented in the numerical results section.

2. Material properties

Fig. 1(a) shows the four types of FG-CNTRC rectangular plates considered in this paper with length *a*, width *b* and thickness *h*. The CNTRC plates considered in this investigation are assumed to be reinforced patterns of carbon nanotube distribution across the plate thickness, which can be seen in Fig. 1(b). Here, three types of FG along with the uniformly distributed case are considered. UD represents the uniform distribution of CNT through the thickness of the matrix and FG-V, FG-O and FG-X denote the functionally graded distributions of CNT through the thickness.

In this research, the modified rule of mixtures approach which contains the efficiency parameters are used extensively to extract the elastic properties of FG-CNTRC plate as Shen (2009).

$$E_{11} = \eta_1 V_{CNT} E_{11}^{CNT} + E^m V_m \tag{1}$$

$$\frac{\eta_2}{E_{22}} = \frac{V_{CNT}}{E_{22}^{CNT}} + \frac{V_m}{E^m} \tag{2}$$

$$\frac{\eta_3}{G_{12}} = \frac{V_{CNT}}{G_{12}^{CNT}} + \frac{V_m}{G^m} \tag{3}$$

where E_{11}^{CNT}, E_{22}^{CNT}, EG_{12}^{CNT} are the Young's and shear modulus of CNT, respectively. G^m, V^m are the Young's modulus and shear modulus of the polymeric matrix. η_1, η_2, η_3 are the CNT efficiency parameters. The volume fraction of CNTs and matrix are denoted by V_{CNT} and V_m, respectively, which can be given by Shen (2009).

$$V_{CNT} + V_m = 1 \tag{4}$$

The effective Poisson's ratio υ and the density ρ of the nanocomposite plates can be determined in the same way as

$$\upsilon_{12} = V_{CNT}\upsilon_{12}^{CNT} + \upsilon_{12}^{CNT}V_m \tag{5}$$

$$\rho = V_{CNT}\rho^{CNT} + \rho^m V_m \tag{6}$$

$$\upsilon_{12} = \upsilon_{13}, \qquad \upsilon_{31} = \upsilon_{21}, \qquad \upsilon_{23} = \upsilon_m \tag{7}$$

where V_{12}^{CNT} and υ^m are the Poisson's ratio and mass density of CNT. As shown in Fig. 1, four types of nanocomposites are investigated in this paper. Therefore, these nanocomposites have unique distribution for the carbon nanotubes which are defined as follow

$$V_{CNT} = \begin{cases} \left(1 + \dfrac{2Z}{h}\right)V_{CNT}^* & \text{(FG-V)} \\ 2\left(1 - \dfrac{2|Z|}{h}\right)V_{CNT}^* & \text{(FG-O)} \\ 2\left(\dfrac{2Z}{h}\right)V_{CNT}^* & \text{(FG-X)} \\ V_{CNT}^* & \text{(UD)} \end{cases} \tag{8}$$

where

$$V_{CNT}^* = \frac{W_{CNT}}{W_{CNT} + \left(\frac{\rho_{CNT}}{\rho_m}\right) - \left(\frac{\rho_{CNT}}{\rho_m}\right)W_{CNT}} \tag{9}$$

It should be mentioned that in this paper $G_{23} = G_{12}$, $G_{13} = G_{12}$. According to Shen (2009), a set of material properties as shown in Table 1.

Table 1 The material properties used in this article

ρ^m	5.6466e^{12}	E_{11}^{CNT}	0.34
ρ^{CNT}	7.98e^{12}	E_{22}^{CNT}	1400
υ^m	1.9445e^{12}	G_{12}^{CNT}	1150
E^m	0.175	υ_{12}^{CNT}	2.5e^9

Remark 1:

The important question that can be asked here is that whether converting nanocomposites with uniformly distributed nanoparticles to functionally graded type has any advantages or not. Experimental tests may answer this question. Nardi *et al.* (2014) studied nanocomposites with polymer matrix and Fe_3O_4-SiO_2 core-shell nanoparticles as reinforcements. In order to synthesis functionally graded nanocomposites, they filled the matrix with core-shell nanoparticles comprising a magnetic core and a silica shell with tailored surface. The magnetic responsive filler is concentrated in specific regions of the composite upon application of magnetic field gradients, ending up with functionally graded distribution in the thickness direction, as shown in Fig. 2. After stating their strategy for synthesis of functionally graded nanocomposites briefly, the results of their work are expressed here. They found that the as-synthesized materials exhibit continuous gradations in mechanical properties and show remarkable increments in elastic modulus (up to 70%) and hardness (up to 150%) when going from particle-depleted to particle-enriched regions. It is mentioned that other research of this team can be found here Nardi *et al.* (2015).

Remark 2:

In this paper, similar to many other papers, modified rule of mixtures method is used for modeling nano-composites. As it has been shown in the literature, classical rule of mixtures method does not predict the mechanical behaviors of nanocomposites accurately and its results has differences with experimental tests especially for high values of volume fractions of CNTs. Same problem can be seen in Halpin-Tsai method, too. So, to overcome this problem, modified rule of mixtures method has been used by many authors. In this modification, some parameters are added to the relations. Then, by calibrating the results

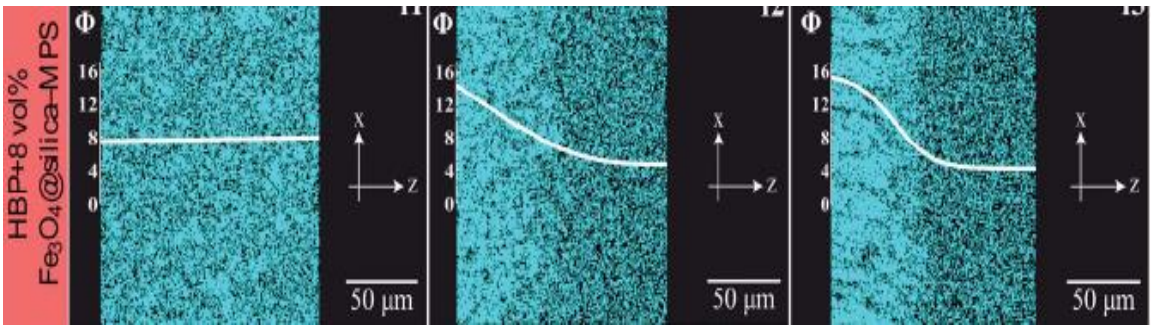

Fig. 2 Cross-sectional SEM-EDX spectral images showing Nardi *et al*. (2014) copyright © (2014) RSC advances

Table 2 The elastic modulus of CNT/epoxy nanocomposites using the Halpin-Tsai equation with different values of the coefficient S (ρ_m = 1100, ρ_f = 1400, AR = 1500, E^f = 700 (Gpa))

Epoxy composites formulation	Matrix modulus E_m (GPa)	Volume fraction V_f (%)	Composites modulus (experimental), E_c (GPa) Zhu *et al*. (2004)	Composites modulus (Halpin-Tsai, S = 3/8) E_c (GPa)	Composites modulus (Halpin-Tsai, S = Eq. (10)) E_c (GPa)
1% SWNTs-R-NH_2	2.026	0.787	2.65	3.733	2.630
4% SWNTs-R-NH_2	2.026	3.17	3.400	8.937	4.510

this relations with experimental data or some other methods such as molecular dynamic simulation, these parameters will be found. The disadvantage of this method may be that it requires the results of experimental tests or other simulation methods. In 2016, Shokrieh and Moshrefzadeh-Sani (2016) presented a modified Halpin-Tsai technique which has not the above disadvantage. In calculating the elastic modulus of randomly oriented composites using Halpin-Tsai method, a constant coefficient exits in the relation. They showed that this coefficient is not constant and depends on the volume fraction and the stiffness ratio of the matrix to reinforcement. According to this point, they derived equations which were able to compute the elastic modulus of both platelet and fibrous randomly oriented composites more accurately as follow with 3-D dispersion of the fibrous reinforcements

$$S = 0.13 + 0.085V_f - 1.669\left(\frac{E^m}{E^f}\right) \tag{10}$$

and with 3-D dispersion of the platelet reinforcements.

$$S = 0.443 - 0.07V_f - 1.468\left(\frac{E^m}{E^f}\right) \tag{11}$$

In above relations *S* can be found here

$$E_c = SE_{11} + (1 - S)E_{22} \tag{12}$$

They made several different comparisons with experimental results on nanocomposites reinforced with CNTs or Graphene Sheets (GSs) and showed that their new relations were accurate. It is noted that although their results are also in a great agreement with experiments but this fact should be considered that all studied cases were performed for nanocomposites with low values of volume fractions of CNTs/GSs. Thus, in Table 2, we make a comparison for a higher value of volume fraction of CNTs, too (wt% = 4%). It can be seen that although the result is more accurate compared to classical Halpin-Tsai but still it has its error. It seems that increasing the volume faction of CNTs leads to unacceptable errors in predicting the modulus of elasticity of nanocomposites based on this method.

3. Constitutive equations

3.1 Review of nonlocal elasticity theory

Eringen (1983) proposed a non-classical model in which the stress at a reference point *x* depends on strain at in a region near that point in other words, the stress tensor at one point is an integral function of the strain tensor at all points in the same area. Accordingly, the structural stress-strain relation for a linear homogeneous elastic material can be expressed as follows

$$\sigma_{ij} = \int_v \alpha\, C_{ijkl}(x')\varepsilon_{kl}(x')dv(x') \tag{13}$$

wherein

$$\alpha = \alpha(|x' - x|, \mu) \tag{14}$$

And the Eringen length parameter ratio is as follows

$$\mu = \frac{e_0 a}{l} \tag{15}$$

herein σ_{ij} and ε_{kl} are local stress tensors and strain tensor at the point $\acute{x}$, respectively; C_{ijkl} is the elastic modulus tensor; and $\alpha = \alpha(|x \acute{-} x|,\mu)$ is the attenuation kernel function whose argument is the Euclidean distance $|x \acute{-} x|$ in which $\mu = e_0 a$ represents nonlocal parameter, a is an internal characteristic length, e_0 is the nonlocal scaling parameter which can be determined such as atomistic simulations or experiments. According to Eringen's nonlocal theory (Eringen 1983), the structural stress-strain relation is defined as follows

$$(1 - \mu^2\nabla^2)\tilde{\sigma}_{ij} = C_{ijkl}\varepsilon_{kl} \tag{16}$$

It is important to note that the main disadvantage of this theory and similar theories is that the exact value of nonlocal parameter for different cases is unknown although several efforts have been done on it. Thus, for industrial usages, we encounter a big problem. Eringen's nonlocal theory has been used in many articles up to now (Raghu *et al*. 2016, Bellal *et al*. 2020, Shiva *et al*. 2019, Asghar *et al*. 2020, Berghouti *et al*. 2019, Taj *et al*. 2020, Hussain *et al*. 2019, Srividhya *et al*. 2018b).

4. Governing equations

Various theories can be used to study nanocomposites (Tounsi *et al*. 2020, Rabhi *et al*. 2020, Bourada *et al*. 2020, Rahmani *et al*. 2020, Bousahla *et al*. 2020, Kaddari *et al*. 2020). In this section, we are going to drive the governing questions for bending and buckling analysis of FG-CNTRC

plates in Cartesian coordinate based on several different higher order theories. The displacement field based on a material point located at (*x*, *y*, *z*) in CNTRC plates is given below (Grover *et al*. 2013)

$$\begin{aligned} u&=u_0(x,y)-z\frac{\delta w_0}{\delta x}+f(z)\theta_x \\ v&=v_0(x,y)-z\frac{\delta w_0}{\delta y}+f(z)\theta_y \\ w&=w_0(x,y) \end{aligned} \tag{17}$$

where u_0, v_0, w_0 are the mid plane displacements, θ_x, θ_y are the shear deformations at the mid plane. By introducing a function $f(z)=g(z)+\Omega Z$ such that $g(z)=sinh^{-1}(rz/h)$ and $\Omega=-2r/\left(h\sqrt{r^2+4}\right)$ also suggest the development of new theories depending upon the accurate choice of shear strain function. The parameter *r* is the transverse shear stress parameter and its value is ascertained by the inverse method in post processing step by comparing the results of the proposed theory and three dimensional elasticity solutions for a wide range of problems and an optimized value is chosen. The parameter Ω is a constant and is evaluated by implementing the transverse shear stress boundary conditions so that the transverse shear stresses at the boundary vanish.

The linear strain-displacement relationship for the in plane and transverse strains can be expressed as

$$\varepsilon_x=\frac{\delta u_0}{\delta x}-z\frac{\partial^2 w_0}{\partial x^2}+f(z)\frac{\delta\theta_x}{\delta x} \tag{18a}$$

$$\varepsilon_y=\frac{\delta v_0}{\delta x}-z\frac{\partial^2 w_0}{\partial y^2}+f(z)\frac{\delta\theta_y}{\delta y} \tag{18b}$$

$$\gamma_{xy}=(\frac{\delta u_0}{\delta y}+\frac{\delta v_0}{\delta x})-z\frac{2\delta^2 w_0}{\delta x\delta y}+[g(z)+\Omega z](\frac{\delta\theta_x}{\delta y}+\frac{\delta\theta_y}{\delta x}) \tag{18c}$$

$$\gamma_{xz}=\frac{-\delta w_0}{\delta x}+f'(z)\theta_x+\frac{\delta w_0}{\delta x}=f'(z)\theta_x \tag{18d}$$

$$\gamma_{yz}=\frac{-\delta w_0}{\delta y}+f'(z)\theta_y+\frac{\delta w_0}{\delta y}=f'(z)\theta_y \tag{18e}$$

where $f(\acute{z})=\acute{g}(z)+\Omega Z$. Since our analysis is on a sandwich nanocomposite plate, we replace the Hook's law with the nonlocal elasticity theory including piezoelectric effects which is defined as follows

$$\begin{Bmatrix}\sigma_x\\ \sigma_y\\ \tau_{xy}\\ \tau_{yz}\\ \tau_{xz}\end{Bmatrix}-\mu\nabla^2\begin{Bmatrix}\sigma_x\\ \sigma_y\\ \tau_{xy}\\ \tau_{yz}\\ \tau_{xz}\end{Bmatrix}=\begin{bmatrix}Q_{11}&Q_{12}&0&0&0\\ Q_{21}&Q_{22}&0&0&0\\ 0&0&Q_{44}&0&0\\ 0&0&0&Q_{55}&0\\ 0&0&0&0&Q_{66}\end{bmatrix} \tag{19}$$
$$=\begin{Bmatrix}\varepsilon_x\\ \varepsilon_y\\ \gamma_{xy}\\ \gamma_{yz}\\ \gamma_{xz}\end{Bmatrix}-\begin{bmatrix}0&0&e_{31}\\ 0&0&e_{32}\\ 0&0&0\\ 0&e_{24}&0\\ e_{15}&0&0\end{bmatrix}\begin{Bmatrix}E_x\\ E_y\\ E_z\end{Bmatrix}$$

where $\mu=(e_0a)^2$ that is nonlocal parameter, and Q_{ij} (1, 2, 3, 4, 5, 6) are the elastic constants given by (Mirzavand and Eslami 2011, Nami *et al*. 2015)

$$\begin{aligned} Q_{11}&=\frac{E_{11}}{(1-\upsilon_{12}\upsilon_{21})}, & Q_{12}&=\frac{E_{11}\upsilon_{21}}{(1-\upsilon_{12}\upsilon_{21})} \\ Q_{22}&=\frac{E_{22}}{(1-\upsilon_{12}\upsilon_{21})}, & Q_{21}&=Q_{12} \\ Q_{44}&=Q_{55}=Q_{66}=G_{12} \end{aligned} \tag{20}$$

Piezoelectric stiffness e_{31}, e_{32}, e_{24}, e_{25} can be considered as the following forms with respect to dielectric constants d_{31}, d_{32}, d_{24}, d_{15} and elastic stiffness c_{ij}^a (i, j = 1, 2, 3, 4, 5, 6) of piezoelectric actuator layers Mirzavand and Eslami (2011).

$$\begin{aligned} e_{31}&=(d_{31}C_{11}^a+d_{32}C_{12}^a) \\ e_{32}&=(d_{31}C_{12}^a+d_{32}C_{22}^a), \\ e_{24}&=d_{24}C_{44}^a \\ e_{15}&=d_{15}C_{55}^a \end{aligned} \tag{21}$$

As transverse electric field component E_z is dominant in the plate type piezoelectric material, it is supposed that

$$E_z=\frac{V_a}{h_a}\ ,\quad E_x=E_y=0 \tag{22}$$

where h_a thickness of piezoelectric layer and V_a is the voltage applied to the actuators in the thickness direction. Equilibrium equations for functionally graded nano-composites based on the theory of nonlocal elasticity are expressed as follows (Grover *et al*. 2013).

$$\frac{\partial N_x}{\partial x}+\frac{\partial N_{xy}}{\partial y}=0 \tag{23a}$$

$$\frac{\partial N_{xy}}{\partial x}+\frac{\partial N_y}{\partial y}=0 \tag{23b}$$

$$\begin{aligned}&\frac{\partial^2 M_x}{\partial x^2}+2\frac{\partial^2 M_{xy}}{\partial x\partial y}+\frac{\partial^2 M_y}{\partial y^2}+q+\tilde{N}_x\frac{\partial^2 w_0}{\partial x^2}\\ &+2\tilde{N}_{xy}\frac{\partial^2 w_0}{\partial x\partial y}+\tilde{N}_y\frac{\partial^2 w_0}{\partial y^2}=0\end{aligned} \tag{23c}$$

$$\Omega\frac{\partial M_x}{\partial x}+\frac{\partial P_x}{\partial x}+\Omega\frac{\partial M_{xy}}{\partial y}+\frac{\partial P_{xy}}{\partial y}-\Omega Q_1-K_1=0 \tag{23d}$$

$$\frac{\partial M_{xy}}{\partial x}+\frac{\partial P_{xy}}{\partial x}+\Omega\frac{\partial M_y}{\partial y}+\frac{\partial P_y}{\partial y}-\Omega Q_2-K_2=0 \tag{23e}$$

Here, resultant stresses, moments are defined as (Grover *et al*. 2013)

$$\begin{aligned}\begin{bmatrix}N_x\\ N_x\\ N_{xy}\end{bmatrix}&=\int_{-\frac{h}{2}-h_a}^{\frac{h}{2}+h_a}\begin{bmatrix}\sigma_x\\ \sigma_y\\ \tau_{xy}\end{bmatrix}\mathrm{dz}\\ \begin{bmatrix}M_x\\ M_y\\ M_{xy}\end{bmatrix}&=\int_{-\frac{h}{2}-h_a}^{\frac{h}{2}+h_a}\begin{bmatrix}\sigma_x\\ \sigma_y\\ \tau_{xy}\end{bmatrix}\mathrm{zdz}\end{aligned} \tag{24}$$

$$\begin{bmatrix} P_x \\ P_y \\ P_{xy} \end{bmatrix} = \int_{-h/2-h_a}^{h/2+h_a} \begin{bmatrix} \sigma_x \\ \sigma_y \\ \tau_{xy} \end{bmatrix} g(z)\mathrm{dz}$$

$$\begin{bmatrix} Q_1 \\ Q_2 \end{bmatrix} = \int_{-\frac{h}{2}-h_a}^{\frac{h}{2}+h_a} \begin{bmatrix} \tau_{xz} \\ \tau_{yz} \end{bmatrix} \mathrm{dz}$$

$$\begin{bmatrix} K_1 \\ K_2 \end{bmatrix} = \int_{-h/2-h_a}^{h/2+h_a} \begin{bmatrix} \tau_{xz} \\ \tau_{yz} \end{bmatrix} g'(z)\mathrm{dz}$$

At this step, to derive the governing equations, the strain-displacement relations are inserted to the constitutive equation to have the stress-displacement relations. Then according to the definitions of stress resultants, the stress resultants will be found in terms of the displacements including a nonlocal parameter. At this step, by combining these relations with the equilibrium equations, the governing equations can be derived. According to this procedure and by defining following integrals

$$\begin{aligned} &\int_{\frac{-h}{2}-h_a}^{\frac{h}{2}+h_a} c_{ij}\, d_z = \mathrm{A}_{ij}, \quad \int_{\frac{-h}{2}-h_a}^{\frac{h}{2}+h_a} c_{ij} z\, d_z = \mathrm{B}_{ij} \\ &\int_{\frac{-h}{2}-h_a}^{\frac{h}{2}+h_a} c_{ij} g(z)\, d_z = D_{ij}, \quad \int_{\frac{-h}{2}-h_a}^{\frac{h}{2}+h_a} c_{ij} z^2\, d_z = \mathrm{F}_{ij} \\ &\int_{\frac{-h}{2}-h_a}^{\frac{h}{2}+h_a} c_{ij} z g(z)\, d_z = \mathrm{G}_{ij}, \quad \int_{\frac{-h}{2}-h_a}^{\frac{h}{2}+h_a} c_{ij} g^2(z)\, d_z = \mathrm{I}_{ij} \\ &\int_{\frac{-h}{2}-h_a}^{\frac{h}{2}+h_a} c_{ij} f'(z)\, d_z = K_{ij}, \quad \int_{\frac{-h}{2}-h_a}^{\frac{h}{2}+h_a} c_{ij} f'(z) g'(z)\, d_z = \mathrm{L}_{ij} \end{aligned} \tag{25}$$

The governing differential equations are expressed under the action of transverse load q, axial compression N_x and N_y and in-plane shear N_{xy} in Eqs. (26)-(30).

$$\begin{aligned} &A_{11}\frac{\partial^2 u_0}{\partial x^2} - B_{11}\frac{\partial^3 w_0}{\partial x^3} + D_{11}\frac{\partial^2 \theta_x}{\partial x^2} + \Omega B_{11}\frac{\partial^2 \theta_x}{\partial x^2} \\ &+ A_{12}\frac{\partial^2 v_0}{\partial y \partial x} - B_{12}\frac{\partial^3 w_0}{\partial y^2 \partial x} + D_{12}\frac{\partial^2 \theta_y}{\partial y \partial x} + \Omega B_{12}\frac{\partial^2 \theta_y}{\partial y \partial x} \\ &+ A_{44}\left(\frac{\partial^2 u_0}{\partial y^2} + \frac{\partial^2 v_0}{\partial x \partial_y}\right) - B_{44}\frac{2\partial^3 w_0}{\partial x \partial y^2} + D_{44}\left(\frac{\partial^2 \theta_x}{\partial y^2}\right. \\ &\left. + \frac{\partial^2 \theta_y}{\partial x \partial_y}\right) + \Omega B_{44}\left(\frac{\partial^2 \theta_x}{\partial y^2} + \frac{\partial^2 \theta_y}{\partial x \partial_y}\right) = 0 \end{aligned} \tag{26}$$

$$\begin{aligned} &A_{44}\left(\frac{\partial^2 u_0}{\partial y \partial_x} + \frac{\partial^2 v_0}{\partial x^2}\right) - B_{44}\frac{2\partial^3 w_0}{\partial x^2 \partial y} + D_{44}\left(\frac{\partial^2 \theta_x}{\partial y \partial_x} + \frac{\partial^2 \theta_y}{\partial x^2}\right) \\ &+ \Omega B_{44}\left(\frac{\partial^2 \theta_x}{\partial y \partial_x} + \frac{\partial^2 \theta_y}{\partial x^2}\right) + A_{21}\frac{\partial^2 u_0}{\partial x \partial_y} - B_{21}\frac{\partial^3 w_0}{\partial x^2 \partial_y} \\ &+ D_{21}\frac{\partial^2 \theta_x}{\partial x \partial_y} + \Omega B_{21}\frac{\partial^2 \theta_x}{\partial x \partial_y} + A_{22}\frac{\partial^2 v_0}{\partial y^2} - B_{22}\frac{\partial^3 w_0}{\partial y^3} \\ &+ D_{22}\frac{\partial^2 \theta_y}{\partial y^2} + \Omega B_{22}\frac{\partial^2 \theta_y}{\partial y^2} = 0 \end{aligned} \tag{27}$$

$$\begin{aligned} &-q - \bar{N}_x\frac{\partial^2 w_0}{\partial x^2} - 2\bar{N}_{xy}\frac{\partial^2 w_0}{\partial x \partial y} - \bar{N}_y\frac{\partial^2 w_0}{\partial y^2} - \mu\nabla^2\left(-q\right. \\ &\left. -\bar{N}_x\frac{\partial^2 w_0}{\partial x^2} - 2\bar{N}_{xy}\frac{\partial^2 w_0}{\partial x \partial y} - \bar{N}_y\frac{\partial^2 w_0}{\partial y^2}\right) = B_{11}\frac{\partial^3 u_0}{\partial x^3} \\ &- F_{11}\frac{\partial^4 w_0}{\partial x^4} + G_{11}\frac{\partial^3 \theta_x}{\partial x^3} + \Omega F_{11}\frac{\partial^3 \theta_x}{\partial x^3} + B_{12}\frac{\partial^3 v_0}{\partial y \partial x^2} \\ &- F_{12}\frac{\partial^4 w_0}{\partial y^2 \partial x^2} + G_{12}\frac{\partial^3 \theta_y}{\partial y \partial x^2} + \Omega F_{12}\frac{\partial^3 \theta_y}{\partial y \partial x^2} + B_{44} \\ &\left(\frac{2\partial^3 u_0}{\partial y^2 \partial x} + \frac{2\partial^3 v_0}{\partial x^2 \partial y}\right) - F_{44}\frac{4\partial^4 w_0}{\partial x^2 \partial y^2} + G_{44}\left(\frac{2\partial^3 \theta_x}{\partial y^2 \partial x}\right. \\ &\left. + \frac{2\partial^3 \theta_y}{\partial x^2 \partial y}\right) + \Omega F_{44}\left(\frac{2\partial^3 \theta_x}{\partial y^2 \partial x} + \frac{2\partial^3 \theta_y}{\partial x^2 \partial y}\right) + B_{21}\frac{\partial^2 u_0}{\partial x \partial y^2} \\ &- F_{21}\frac{\partial^4 w_0}{\partial x^2 \partial y^2} + G_{21}\frac{\partial^3 \theta_x}{\partial x \partial y^2} + \Omega F_{21}\frac{\partial^3 \theta_x}{\partial x \partial y^2} + B_{22}\frac{\partial^3 v_0}{\partial y^3} \\ &- F_{22}\frac{\partial^4 w_0}{\partial y^4} + G_{22}\frac{\partial^3 \theta_y}{\partial y^3} + \Omega F_{22}\frac{\partial^3 \theta_y}{\partial y^3} \end{aligned}$$

$$\begin{aligned} &(B_{11}\Omega + D_{11})\frac{\partial^2 u_0}{\partial x^2} - (F_{11}\Omega + G_{11})\frac{\partial^3 w_0}{\partial x^3} + (G_{11}\Omega \\ &+ I_{11})\frac{\partial^2 \theta_x}{\partial x^2} + (\Omega^2 F_{11} + \Omega G_{11})\frac{\partial^2 \theta_x}{\partial x^2} + (B_{12}\Omega + D_{12}) \\ &\frac{\partial^2 v_0}{\partial y \partial x} - (F_{12}\Omega + G_{12})\frac{\partial^3 w_0}{\partial y^2 \partial x} + (G_{12}\Omega + I_{12})\frac{\partial^2 \theta_y}{\partial y \partial x} + \\ &(\Omega^2 F_{12} + \Omega G_{12})\frac{\partial^2 \theta_y}{\partial y \partial x} + (\Omega B_{44} + D_{44})\left(\frac{\partial^2 u_0}{\partial y^2} + \frac{\partial^2 v_0}{\partial x \partial y}\right) \\ &-(\Omega F_{44} + G_{44})\frac{2\partial^3 w_0}{\partial x \partial y^2} + (\Omega G_{44} + I_{44})\left(\frac{\partial^2 \theta_x}{\partial y^2} + \frac{\partial^2 \theta_y}{\partial x \partial y}\right) \\ &+(\Omega^2 F_{44} + \Omega G_{44})\left(\frac{\partial^2 \theta_x}{\partial y^2} + \frac{\partial^2 \theta_y}{\partial x \partial y}\right) - (\Omega K_{66} + L_{66})\theta_x = 0 \end{aligned} \tag{29}$$

$$\begin{aligned} &(\Omega B_{44} + D_{44})\left(\frac{\partial^2 u_0}{\partial y \partial x} + \frac{\partial v_0}{\partial x^2}\right) - (\Omega F_{44} + G_{44})\frac{2\partial^3 w_0}{\partial x^2 \partial y} + \\ &(\Omega G_{44} + I_{44})\left(\frac{\partial^2 \theta_x}{\partial y \partial x} + \frac{\partial^2 \theta_y}{\partial x^2}\right) + (\Omega^2 F_{44} + \Omega G_{44})\left(\frac{\partial^2 \theta_x}{\partial y \partial x}\right. \\ &\left. + \frac{\partial^2 \theta_y}{\partial x^2}\right) + (\Omega B_{21} + D_{21})\frac{\partial^2 u_0}{\partial x \partial y} - (\Omega F_{21} + G_{21})\frac{\partial^3 w_0}{\partial x^2 \partial y} \\ &+ (\Omega G_{21} + I_{21})\frac{\partial^2 \theta_x}{\partial x \partial y} + (\Omega^2 F_{21} + \Omega G_{21})\frac{\partial^2 \theta_x}{\partial x \partial y} + (\Omega B_{22} \\ &+ D_{22})\frac{\partial^2 v_0}{\partial y^2} - (\Omega F_{22} + G_{22})\frac{\partial^3 w_0}{\partial y^3} + (\Omega G_{22} + I_{22})\frac{\partial^2 \theta_y}{\partial y^2} \\ &+ (\Omega^2 F_{22} + \Omega G_{22})\frac{\partial^2 \theta_y}{\partial y^2} - (\Omega K_{55} + L_{55})\theta_y = 0 \end{aligned} \tag{30}$$

5. Solution methodology

Since the simplicity of the method of solution is desirable in engineering applications, the obtained differential equations can be solved analytically with simple trigonometric terms. Here, the Navier method is employed to present the solutions for bending and buckling problems of simply supported CNTRC plates having length *an* and width *b*. trigonometric terms for approximating the displacements can be expressed as follows

$$u_0 = \sum_{m=1}^{\infty}\sum_{n=1}^{\infty} U_{mn}\cos(\alpha x)\, sin(\beta y) \tag{31a}$$

$$u_0 = \sum_{m=1}^{\infty}\sum_{n=1}^{\infty} V_{mn}\cos(\alpha x)\, sin(\beta y) \tag{31b}$$

$$w_0 = \sum_{m=1}^{\infty}\sum_{n=1}^{\infty} W_{mn} \sin(\alpha x)\, sin(\beta y) \quad (31c)$$

$$\theta_x = \sum_{m=1}^{\infty}\sum_{n=1}^{\infty} X_{mn} \cos(\alpha x)\, sin(\beta y) \quad (31d)$$

$$\theta_y = \sum_{m=1}^{\infty}\sum_{n=1}^{\infty} Y_{mn} \sin(\alpha x)\, cos(\beta y) \quad (31e)$$

where $\alpha = \frac{m\pi}{a}$ and $\beta = \frac{n\pi}{b}$. For the mechanical load, q (x, y) is also expanded in double Fourier sine series as follows

$$q = \sum_{m=1}^{\infty}\sum_{n=1}^{\infty} Q_0\, sin(\alpha x)\, sin(\beta y) \quad (32)$$

where $Q_0 = \frac{16q_0}{mn\pi}$. As the last step, by inserting Eqs. (28a)-(28e) approximation in Eqs. (26)-(30), one can easily study the bending and buckling analysis of FG-CNTRC plate with simply supported edge condition. A closed-form solution for the buckling analysis of FG-CNTRC plate is also presented in the appendix.

6. Numerical results and discussions

The computer package MATLAB is used to code the expressions obtained above to calculate the deflections and buckling loads for functionally graded carbon nanotube-reinforced rectangular composite plates. It is noted that although our study is on FG nanocomposite but to show the accuracy of our work, our results are compared for nanoplates. For this purpose, our results are compared with the numerical results available in literature, as shown in Table 3. In this table, the deflections of rectangular nanoplate are compared with the methodology presented by Nami and Janghorban (2014b) for different nonlocal parameters. It is seen that our results are in great agreement with them so we can assure that our formulation and the return code are correct. Another verification is done for critical buckling loads of simply supported rectangular nanoplate in Table 4. The buckling loads are compared with the methodology presented by Nami and Janghorban (2015b). From this table, it is understood that the results are verified well for several length scale parameters. In this Comparison it's noted that E = 1060e^9, b = 2, ν = 0.3, a = 1. It is also seen that with the increase of nonlocal parameter the critical buckling loads decrease.

To verify the present formulation, several comparison studies are carried out in Table 5 for the simply supported FG-CNTRC plate subjected to a uniform load ($\overline{w} = -w_0/h$) which shows the comparison of the non-dimensional central deflection (a = b, V_{CNT}^{*} = 11%). Three types of distributions of carbon nanotubes along the thickness direction are considered: UD, FG-O and FG-X. In this table, the present formulation method is compared with those reported by Duc *et al*. (2017), Phung-Van *et al*. (2015), Zhu *et al*. (2012b) and the material properties at room temperature (T_0 = 300 K) are (Duc *et al*. 2017): ν_m =

Table 3 Comparison the deflections of rectangular nanoplates

		a/h		
μ	Theory	10	20	50
0	Nami and Janghorban (2014a)	1.097e^{-10}	8.778e^{-10}	1.371e^{-8}
	Present	1.095e^{-10}	8.775e^{-10}	1.371e^{-8}
0.5	Nami and Janghorban (2014a)	7.865e^{-10}	6.292e^{-9}	9.832e^{-8}
	Present	7.852e^{-10}	6.290e^{-9}	9.831e^{-8}
1	Nami and Janghorban (2014a)	1.463e^{-9}	1.170e^{-8}	1.829e^{-7}
	Present	1.461e^{-9}	1.170e^{-8}	1.829e^{-7}
2	Nami and Janghorban (2014a)	2.817e^{-9}	2.253e^{-8}	3.521e^{-7}
	Present	2.812e^{-9}	2.252e^{-8}	3.521e^{-7}

Table 4 Comparison the buckling loads of rectangular nanoplates

		a/h		
μ	Theory	10	20	50
0	Nami and Janghorban (2015a)	1.499e^9	1.854e^8	1.195e^7
	Present	1.446e^9	1.871e^8	1.197e^7
0.5	Nami and Janghorban (2015a)	2.017e^8	2.587e^7	1.668e^6
	Present	2.091e^8	2.611e^7	1.670e^6
1	Nami and Janghorban (2015a)	1.084e^8	1.390e^7	896655
	Present	1.124e^8	1.403e^7	897966
2	Nami and Janghorban (2015a)	5.632e^7	7.224e^6	465799
	Present	5.840e^7	7.290e^6	466477

Table 5 Comparison the central deflection for the simply supported FG-CNTRC plate

h/a	Types	Present	Duc *et al*. (2017)	Phung-Van *et al*. (2015)	Zhu *et al*. (2012a)
0.02	UD	1.2669	1.2853	1.1630	1.1550
	FG-O	2.3157	2.3403	2.2001	2.1570
	FG-X	0.87833	0.8947	0.7877	0.7900
0.05	UD	3.684e^{-02}	3.907e^{-02}	3.564e^{-02}	3.628e^{-02}
	FG-O	6.423e^{-02}	6.569e^{-02}	6.170e^{-02}	6.155e^{-02}
	FG-X	2.684e^{-02}	2.917e^{-02}	2.591e^{-02}	2.701e^{-02}

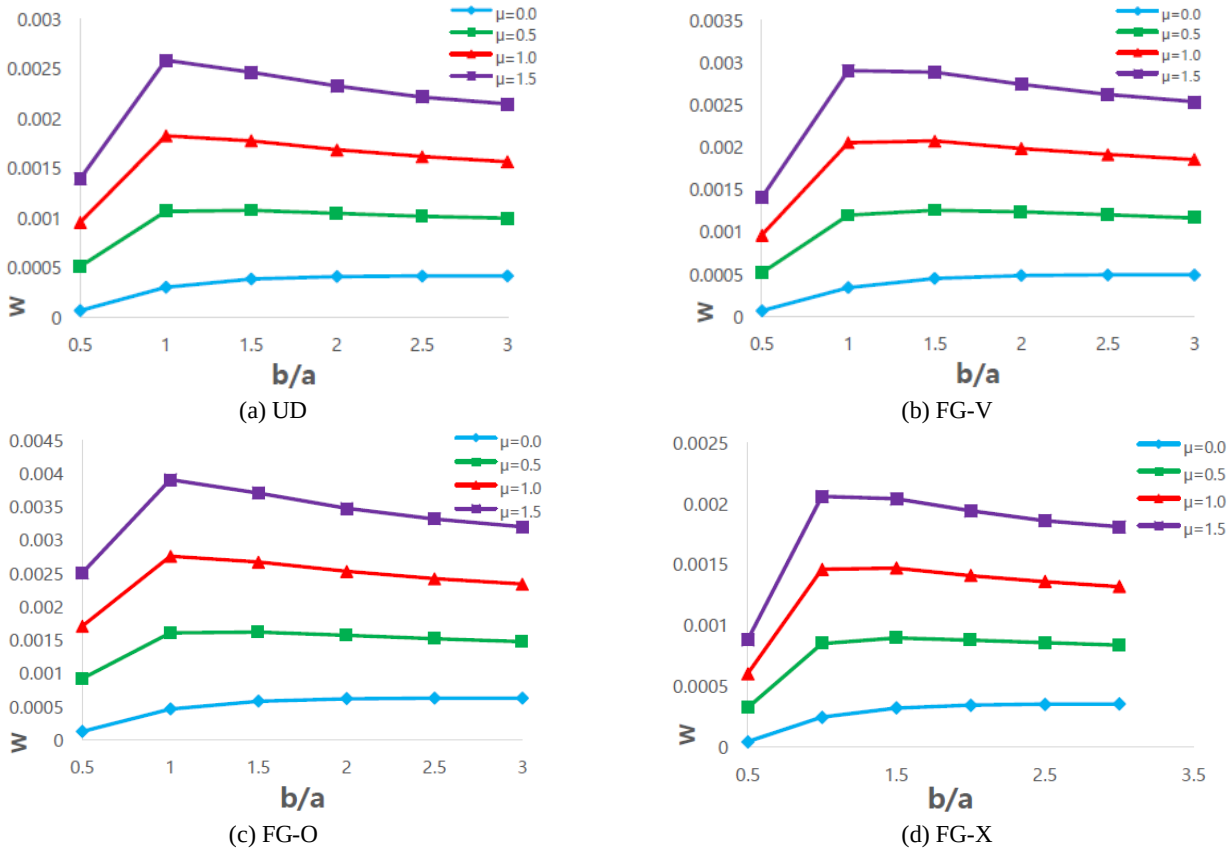

(a) UD (b) FG-V

(c) FG-O (d) FG-X

Fig. 3 Effects of variations of aspect ratio and nonlocal parameter on the deflections of functionally graded nanocomposite plates (a/h = 10; b = 1, 2, …)

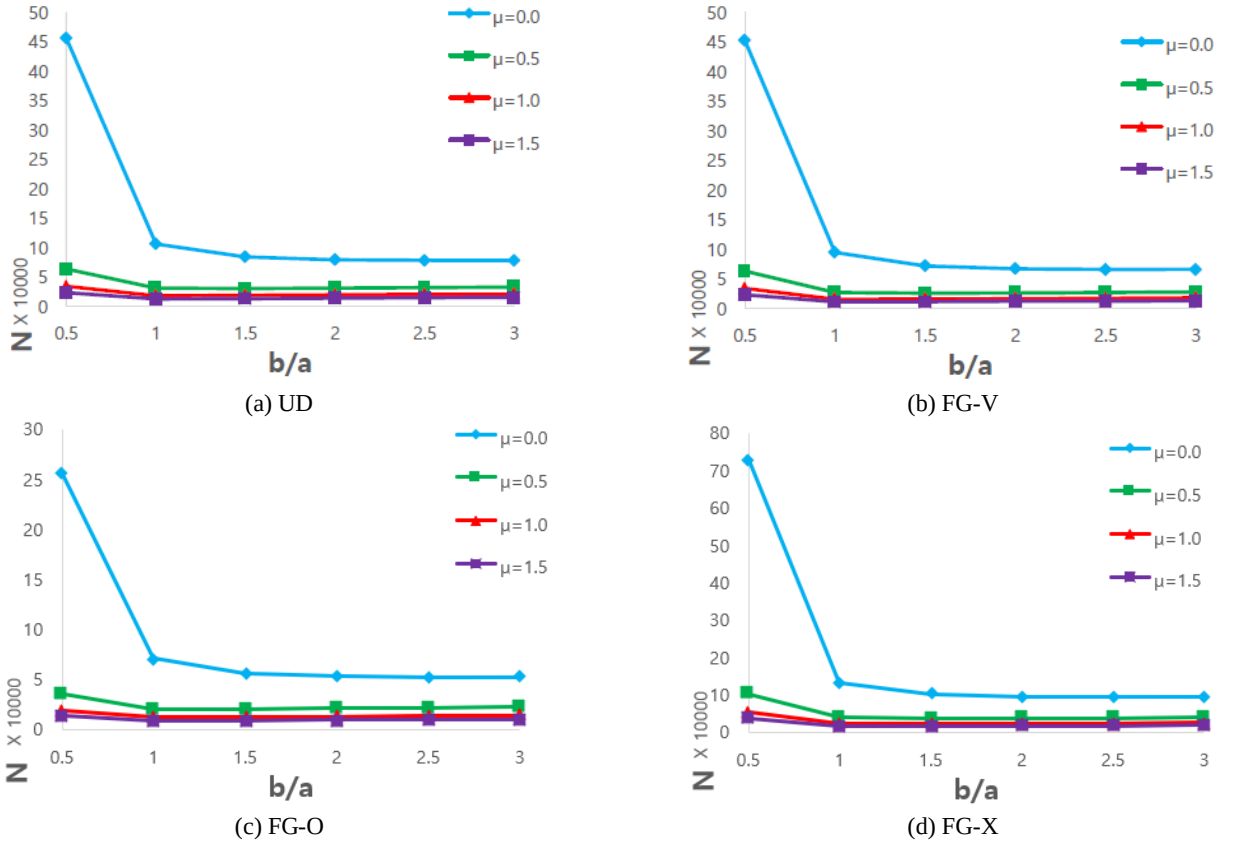

(a) UD (b) FG-V

(c) FG-O (d) FG-X

Fig. 4 Effect of change the size on buckling of functionally graded nanocomposite plates (a/h = 10; b = 1, 2,…, 6; h = 0.2)

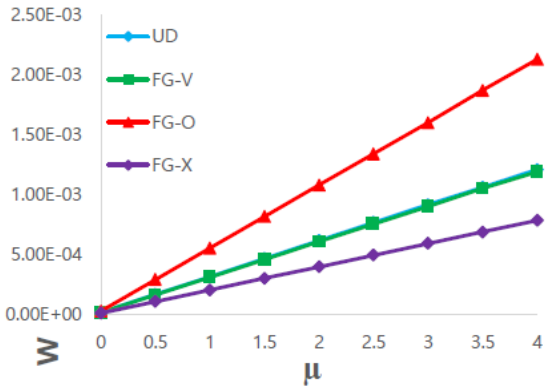

(a) a/h = 5

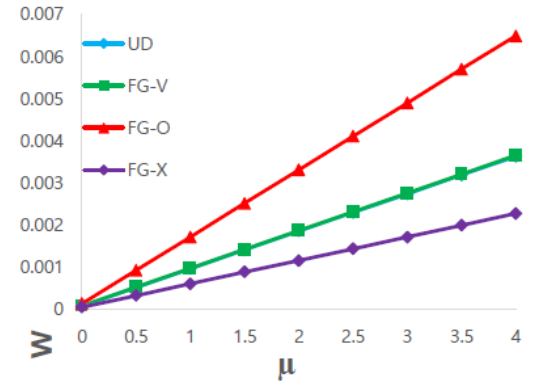

(b) a/h = 10

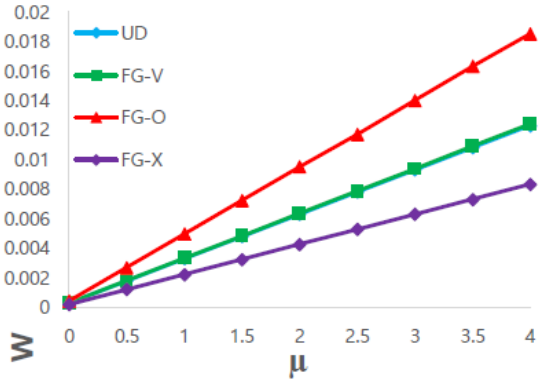

(c) a/h = 20

Fig. 5 The effects of nonlocal parameter and length to thickness ratio on the deflections (h = 0.2; b = 1)

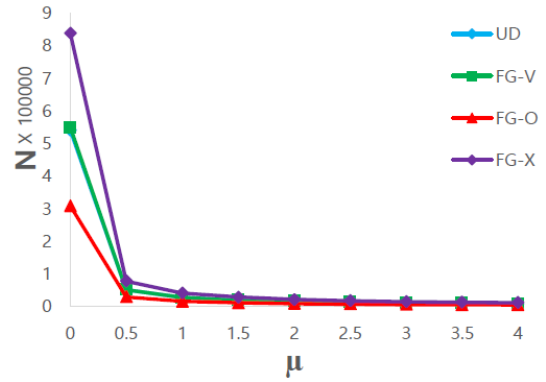

(a) a/h = 5

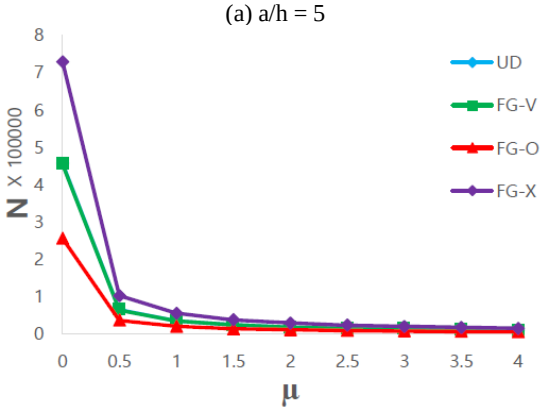

(b) a/h = 10

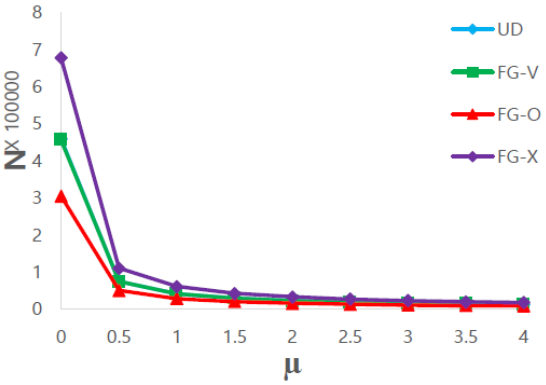

(c) a/h = 20

Fig. 6 The effects of nonlocal parameter and length to thickness ratio on the buckling (μ = 0, 0.5, 1, …, 4; h = 0.2; b = 1)

0.34 , $\rho_m = 1150\,Kg/m^3$, $E_m =$ 2.1 GPa, $E_{11}^{CNT} =$ 5.6466 (TPa), $E_{22}^{CNT} = 7.08$ (TPa) and $G_{12}^{CNT} = 31.9445$ (TPa). The CNT efficiency parameters are $\eta_1 = 0.149$, $\eta_2 = 0.934$ for the case $V_{CNT}^{*} = 11\%$ and note that $\eta_2 = \eta_3$, $G_{23} = G_{13} = G_{12}$.

In Fig. 3, the deflections of both types of nano-composites with uniform and non-uniform nanotube distributions are considered. As can be seen in this figure for uniformly distributed and all types of functionally graded nanocomposites, in almost all cases, the deflections increase and then decrease by converging to a certain value with the increase of aspect ratio. It is worth noting that in all four studied cases, for high aspect ratios, no further changes can be seen in the deflections of nanocomposites. Above conclusions occur for almost all nonlocal values. It is also seen from the results that with increasing nonlocal parameter, the deflections of nanocomposites rise in all cases. The reason for this phenomena is that increasing the nonlocal parameter decreases the stiffness of the nanocomposite and consequently, increases the plate deflection.

In Fig. 4, both nanocomposites with uniformly and non-uniformly distributed nanotubes are considered. As can be seen in the figure, for UD, FG-V, FG-O and FG-X nanocomposites, the critical buckling force decrease and then stays constant with increasing the aspect ratio of the of the nanocomposite and then it converges to a certain value. It is worth noting that in all four studied cases, for high values of aspect ratios, we no longer see any changes in the

Table 6 Equivalence of various shear deformation theories

Theory	g(z)	Ω
Model 1 Grover *et al*. (2013)	$sinh^{-1}\left(\frac{rz}{h}\right)$	$\frac{-2}{r\sqrt{r^2+4}}$ $r = 3.0$
Model 2 Reddy (1984)	$\left(z-\frac{4z^3}{3h^2}\right)$	0
Model 3 Touratier (1991)	$\frac{h}{\pi}sin\left(\frac{\pi z}{h}\right)$	0
Model 4 Mantari *et al*. (2012)	$sin\left(\frac{\pi z}{h}\right)$	$\frac{\pi}{2h}$
Model 5 Singh and Sigh (2017)	$sin\left(\frac{2\pi r}{h}\right)z$	$\frac{r\pi}{h}$ $r = 0.5$
Model 6 Ambartsumian (1958)	$\frac{z}{2}\left[\frac{h^2}{4}-\frac{z^2}{3}\right]$	0
Model 7 Mantari *et al*. (2011)	$z2\cdot 85^{-2(z/h)^2}+rz$	$r = 0.028$
Model 8 Kaczkowski (1968), Panc (1975), Reissner (1975)	$\frac{5z}{4}\left[1-\frac{4z^2}{3h^2}\right]$	0

Table 7 Comparing the results of eight different models for the bending analysis of thick FG-CNTRC

a/h = 5		UD	FG-V	FG-O	FG-X
μ = 0.5	Model 1	0.000402	0.000430	0.000541	0.000364
	Model 2	0.000405	0.000439	0.000477	0.000377
	Model 3	0.000443	0.000478	0.000575	0.000408
	Model 4	0.000445	0.000480	0.000575	0.000410
	Model 5	0.000414	0.000452	0.000488	0.000386
	Model 6	0.000448	0.000483	0.000573	0.000414
	Model 7	0.000436	0.000471	0.000575	0.000399
	Model 8	0.000448	0.000483	0.000573	0.000414
μ = 1.0	Model 1	0.000737	0.000789	0.000992	0.000668
	Model 2	0.000743	0.000806	0.000875	0.000693
	Model 3	0.000813	0.000878	0.00105	0.000748
	Model 4	0.000816	0.000881	0.00105	0.000752
	Model 5	0.000759	0.000829	0.000895	0.000708
	Model 6	0.000823	0.000887	0.00105	0.000760
	Model 7	0.000800	0.000865	0.00105	0.000732
	Model 8	0.000823	0.000887	0.00105	0.000760
μ = 2.0	Model 1	0.00140	0.00150	0.00189	0.00127
	Model 2	0.00142	0.00154	0.00167	0.00132
	Model 3	0.00155	0.00167	0.00201	0.00142
	Model 4	0.00155	0.00168	0.00201	0.00143
	Model 5	0.00145	0.00158	0.00171	0.00135
	Model 6	0.00157	0.00169	0.00200	0.00145
	Model 7	0.00152	0.00165	0.00201	0.00139
	Model 8	0.00157	0.00169	0.00200	0.00145

critical buckling force of the nanocomposites. The above

Table 8 Comparing the results of eight different models for the bending analysis of moderately thick FG-CNTRC

a/h = 5		UD	FG-V	FG-O	FG-X
μ = 0.5	Model 1	0.000977	0.00114	0.00144	0.000823
	Model 2	0.000990	0.00120	0.00144	0.000829
	Model 3	0.00107	0.00129	0.00160	0.000912
	Model 4	0.00108	0.00130	0.00160	0.000914
	Model 5	0.00102	0.00127	0.00152	0.000858
	Model 6	0.00108	0.00130	0.00159	0.000916
	Model 7	0.00108	0.00129	0.00161	0.000906
	Model 8	0.00108	0.00130	0.00159	0.000916
μ = 1.0	Model 1	0.00153	0.00180	0.00226	0.00129
	Model 2	0.00155	0.00190	0.00226	0.00130
	Model 3	0.00169	0.00204	0.00252	0.00143
	Model 4	0.00169	0.00204	0.00252	0.00143
	Model 5	0.00161	0.00200	0.00239	0.00134
	Model 6	0.00170	0.00204	0.00251	0.00144
	Model 7	0.00169	0.00203	0.00253	0.00142
	Model 8	0.00170	0.00204	0.00251	0.00144
μ = 2.0	Model 1	0.00265	0.00311	0.00391	0.00223
	Model 2	0.00268	0.00328	0.00391	0.00225
	Model 3	0.00292	0.00352	0.00435	0.00247
	Model 4	0.00293	0.00353	0.00436	0.00248
	Model 5	0.00274	0.00346	0.00412	0.00233
	Model 6	0.00293	0.00353	0.00434	0.00248
	Model 7	0.00291	0.00352	0.00438	0.00246
	Model 8	0.00293	0.00353	0.00434	0.00248

results are true for all nonlocal values. It is also seen from the results that with increasing the nonlocal parameter, a decreasing trend can be seen in critical buckling force of nanocomposites in all cases because of a reduction in the stiffness of the nanocomposite plates. It is mentioned that same behaviors can be seen in Fig. 4 of Lei *et al*. (2013).

In Fig. 5, the effects of nonlocal parameter and thickness ratio are studied on the bending behavior of different types of functionally graded rectangular nanocomposites reinforced with nanotubes. It is seen that with the increase of nonlocal parameter the deflections also increase for all types of FG nanocomposites. The reason of this phenomenon is that the stiffness of FG nanocomposites decreases with the increase of nonlocal parameter. It is noted that the results of UD and FG-V are very close to each other in this figure. So, only three lines can be seen in the figure. It is also shown that FG-O type has the highest deflections in studied cases. Therefore, it has the lowest stiffness. This result is not dependent on the values of nonlocal parameter.

In Fig. 6, the influences of length scale parameter and thickness ratio are studied on the buckling behavior of different types of functionally graded rectangular nanocomposites. From this figure, it is seen that with increasing the nonlocality, the critical buckling force

Table 9 Comparing the results of eight different models for the critical buckling loads analysis of thick FG-CNTRC

a/h = 5		UD	FG-V	FG-O	FG-X
μ = 0.5	Model 1	20425.627	19141.337	15179.267	22523.028
	Model 2	20251.488	18727.168	17199.204	21737.302
	Model 3	18515.758	17199.937	14281.659	20125.519
	Model 4	18444.164	17135.609	14282.637	20017.364
	Model 5	19834.010	18216.497	16821.768	21252.152
	Model 6	18299.741	16931.127	14326.074	19808.850
	Model 7	18821.764	17451.373	14263.741	20557.175
	Model 8	18299.741	16983.697	14326.074	19808.850
μ = 1.0	Model 1	11135.295	10435.147	8278.173	12278.720
	Model 2	11040.360	10209.358	9376.368	11850.371
	Model 3	10094.105	9376.768	7785.831	10971.687
	Model 4	10055.075	9341.699	7786.364	10912.725
	Model 5	10812.767	9930.959	9170.604	11585.885
	Model 6	9976.340	9230.223	7810.045	10799.050
	Model 7	10260.928	9513.842	7776.062	11207.010
	Model 8	9976.340	9258.882	7810.045	10799.050
μ = 2.0	Model 1	5830.992	5464.360	4333.291	6429.746
	Model 2	5781.279	5346.125	4909.931	6205.441
	Model 3	5285.773	4910.140	4077.047	5745.319
	Model 4	5265.335	4891.776	4077.326	5714.443
	Model 5	5662.100	5200.342	4802.183	6066.943
	Model 6	5224.106	4833.402	4089.726	5654.918
	Model 7	5373.130	4981.919	4071.931	5868.545
	Model 8	5224.106	4848.409	4089.726	5654.918

Table 10 Comparing the results of eight different models for the critical buckling loads analysis of moderately thick FG-CNTRC

a/h = 5		UD	FG-V	FG-O	FG-X
μ = 0.5	Model 1	33596.592	28673.638	22766.233	39915.659
	Model 2	33170.563	27181.246	22804.479	39616.775
	Model 3	30444.095	25298.628	20466.265	36008.703
	Model 4	30383.768	25241.025	20451.227	35914.908
	Model 5	31921.264	25740.728	21598.000	38256.816
	Model 6	30363.844	25227.151	20544.803	35833.938
	Model 7	30363.844	25343.276	20359.868	36245.404
	Model 8	30363.844	25238.669	20544.803	35833.938
μ = 1.0	Model 1	21376.959	18244.564	14485.779	25397.677
	Model 2	21105.883	17294.980	14510.115	25207.502
	Model 3	19371.076	16097.100	13022.348	22911.745
	Model 4	19332.691	16060.449	13012.779	22852.065
	Model 5	20310.975	16378.401	13743.039	24342.182
	Model 6	19320.014	16051.621	13072.320	22800.545
	Model 7	19438.068	16125.509	12954.648	23062.354
	Model 8	19320.014	16058.949	13072.320	22800.545
μ = 2.0	Model 1	12374.986	10561.662	8385.726	14702.554
	Model 2	12218.062	10011.954	8399.813	14592.463
	Model 3	11213.793	9318.509	7538.555	13263.464
	Model 4	11191.573	9297.292	7533.015	13228.916
	Model 5	11754.895	9481.353	7955.758	14091.535
	Model 6	11184.234	9292.182	7567.483	13199.091
	Model 7	11252.575	9334.955	7499.364	13350.651
	Model 8	11184.234	9296.424	7567.483	13199.091

decreases and then converges to a certain value for all types of FG nanocomposites. The reason of this phenomenon can be also related to the stiffness of nanocomposites. It is mentioned that the critical buckling loads of UD and FG-V are very close to each other in this figure so only three lines can be seen. In this figure it is also shown that FG-X type has the highest buckling loads so it has the lowest stiffness. This result is independent of the values of length scale parameter.

In last decade, several different plate theories be having been derived up to now. Some of them have some novelties although unfortunately several others have nothing new. In present paper we are going to compare the results of some of these theories for static and buckling analysis of FG-nanocomposites. The differences of these theories can be seen in a function $f(z)$. This function is defined in Table 6. In this article, we will examine 8 different higher order shear deformation theories for studying bending and buckling behavior of FG-CNTRC including size effects.

In Tables 7 and 8, we study the bending behaviors of FG-CNTRC nanocomposites versus the variations of nonlocal parameter and length to thickness ratio. Different types of FG nanocomposites and displacement fields are considered for this purpose. It can be seen from these tables that for thick and moderately thick nanocomposites, FG-O presents the highest and FG-X presents the lowest value for deflection. This conclusion is not related to the values of nonlocal parameter. It is mention that the results of models 6 and 8 are almost the same in all cases. By comparing the models with each other, one can see that for all types of FG-CNTRC nanocomposites, the values of deflection in models 3, 4, 6, 7 and 8 are very close to each other. From these tables one can find that model 1 and then model 2 predicts the lowest value for deflection in all cases. It is also shown that with increasing the nonlocal parameter and length to thickness ratio, the bending value also increases in all models.

In Tables 9 and 10, the influences of nonlocal parameter and length to thickness ratio on the critical buckling load of FG-CNTRC nanocomposites are investigated. Various types of FG nanocomposites and plate models are adopted in this study. From these tables one can understand that for thick and moderately thin nanocomposites, FG-X has the highest critical buckling load and it occurs in Model 1. Also, FG-O has the lowest value for buckling loads and it occurs in Model 7. These results are not dependent nonlocality. It is found from these tables that by increasing the nonlocal parameter and length to thickness ratio, the critical buckling

Table 11 The influences of piezoelectric layers on the bending behavior of FG-CNTRC ($\frac{a}{h} = 10$, b = 1, 2,…,6, h = 0.2, h_a = 0.002)

μ	UD		FG-V		FG-O		FG-X	
	$h_a = 0$	$h_a \neq 0$	$h_a = 0$	$h_a \neq 0$	$h_a = 0$	$h_a \neq 0$	$h_a = 0$	$h_a \neq 0$
μ = 0	0.0000720	0.0000687	0.0000725	0.0000690	0.000128	0.000123	0.0000451	0.000427
	0.000308	0.000300	0.000347	0.000337	0.000465	0.000452	0.000246	0.000239
	0.000390	0.000381	0.000456	0.000445	0.000585	0.000570	0.000322	0.000315
	0.000414	0.000405	0.000489	0.000477	0.000620	0.000605	0.000345	0.000338
	0.000421	0.000412	0.000498	0.000486	0.000628	0.000614	0.000352	0.000346
	0.000421	0.000412	0.000497	0.000485	0.000626	0.000611	0.000354	0.000347
μ = 0.5	0.000516	0.000492	0.000520	0.000495	0.000923	0.00887	0.000323	0.00306
	0.00107	0.00104	0.00120	0.00116	0.00161	0.00157	0.000852	0.000830
	0.00108	0.00106	0.00126	0.00123	0.00162	0.00158	0.000897	0.000878
	0.00105	0.00103	0.00124	0.00121	0.00157	0.00153	0.000878	0.000861
	0.00102	0.00100	0.00121	0.00118	0.00152	0.00149	0.000857	0.000841
	0.000999	0.000978	0.00117	0.00115	0.00148	0.00145	0.000839	0.000823
μ = 1	0.000961	0.000916	0.000967	0.000921	0.00171	0.00165	0.000602	0.000570
	0.00183	0.00178	0.00206	0.00200	0.00276	0.00268	0.00146	0.00142
	0.00178	0.00174	0.00208	0.00203	0.00267	0.00260	0.00147	0.00144
	0.00169	0.00165	0.00199	0.00195	0.00253	0.00247	0.00141	0.00138
	0.00162	0.00159	0.00192	0.00187	0.00242	0.00237	0.00136	0.00133
	0.00157	0.00154	0.00186	0.00181	0.00234	0.00228	0.00132	0.00129

Table 12 The influences of piezoelectric layers on the critical buckling loads behavior of FG-CNTRC ($\frac{a}{h} = 10$, b = 1, 2,…,6, h = 0.2, h_a = 0.002)

μ	UD		FG-V		FG-O		FG-X	
	$h_a = 0$	$h_a \neq 0$	$h_a = 0$	$h_a \neq 0$	$h_a = 0$	$h_a \neq 0$	$h_a = 0$	$h_a \neq 0$
μ = 0	455791.658	478037.016	453105.501	475972.948	254924.489	265398.751	727772.156	768641.655
	106324.317	109188.061	94708.376	97488.699	70592.645	72551.435	133539.181	137183.260
	84142.636	86046.170	72078.047	73873.110	56150.799	57537.510	101799.197	103995.992
	79308.148	81016.559	67217.782	68815.635	52905.772	54235.241	95064.059	96975.984
	77983.760	79643.750	65999.566	67553.551	52240.994	53490.055	93108.188	94942.899
	77897.662	79559.998	66112.307	67677.531	52445.384	53710.854	92761.224	94586.451
μ = 0.5	63582.546	66685.754	63207.829	66397.818	35561.748	37022.898	101523.593	107224.853
	30663.979	31489.884	27313.937	28115.783	20358.950	20923.865	38512.758	39563.712
	30245.246	30929.476	25908.604	26553.843	20183.522	20681.978	36591.934	37381.576
	31197.571	31869.612	26441.565	27070.115	20835.229	21334.602	37395.499	38147.596
	32077.658	32760.475	27148.108	27787.321	21488.689	22002.475	38298.905	39053.591
	32857.420	33558.597	27886.329	28546.544	22121.588	22655.367	39126.906	39896.791
μ = 1	34174.962	35842.904	33973.555	35688.142	19114.072	19899.425	54567.883	57632.251
	17915.393	18397.927	15958.135	16426.613	11894.692	12224.473	22501.033	23115.051
	18436.064	18853.138	15792.653	16185.960	12302.915	12606.750	22304.703	22786.031
	19418.037	19836.330	16457.797	16849.020	12968.294	13279.114	23275.761	23743.882
	20191.615	20621.421	17088.658	17491.017	13526.278	13849.686	24107.644	24582.689
	20819.585	21263.875	17669.732	18088.067	14016.995	14355.215	24792.146	25279.972

load decrease in all predicted models. Moreover, one can understand that in UD, FG-V, FG-O and FG-X, the predicted values of buckling load are very close to each other in models 3, 4, 6, 7 and 8.

One of the goals of this paper is studying the effects of piezoelectric layers on the behavior of FG nanocomposites. In Tables 11 and 12, we investigate the behaviors of bending and buckling analysis in the presence of piezoelectric layers. As can be seen, for each of the four cases, with the addition of piezoelectric layers, for all values of the nonlocal parameters, the bending values are getting bigger and the critical buckling loads are getting smaller. It is also observed that by increasing the aspect ratio and nonlocal parameter, with or without piezoelectric layer and without piezoelectric layers, the deflections increase and the buckling loads decrease.

7. Conclusions

An analytical solution was obtained for the bending and buckling analysis of simply supported functionally graded rectangular nanocomposites reinforced with carbon nanotubes including piezoelectric layers and nonlocality using a higher order theory with eight different displacement fields. In present paper, four kinds of functionally graded nanocomposites were investigated: (1) UD, (2) FG-V, (3) FG-O, (4) FG-X. The effects of different parameters such as different displacement fields, nonlocal parameter and piezoelectric layers were also studied. The reliability of the present approach was verified by comparing the obtained results with those provided in literature. It is mentioned that one of the interesting points in this article was presenting real images of FG-CNTRCs and a brief review of the synthesis method of FG-CNTRCs. Relying on the numerical results section of the present research, the following considerations are seen:

• With the increase of length to thickness ratio, the deflections of FG-CNTRC will increase and critical buckling load decrease.

• Increasing the nonlocal parameter which causes the critical buckling force of the FG-CNTRC to decrease, will increase the deflections.

• It seems that in our model for FG-CNTRCs with piezoelectric layers, length to thickness ratio has more effect in comparison with nonlocal parameter.

• Effects of nonlocal parameter depend on aspect ratios.

• The presence of piezoelectric layers in our model leads to an increase in the critical buckling force and a reduction in the bending of FG-CNTRC.

• It seems that in our model for FG-CNTRC with piezoelectric layers, the nonlocal parameter has less effect in comparison with length to thickness ratio.

• For the given material properties, the influences of distributions of CNTs on the results increase with decreasing the nonlocal parameter.

References

Al-Nemrawi, N.K., AbuAlSamen, M.M. and Alzoubi, K.H. (2019), "Awareness about nanotechnology and its applications in drug industry among pharmacy students", *Curr. Pharm. Teach. Learn.*, **12**(3), 274-280. https://doi.org/10.1016/j.cptl.2019.12.003.

Alimirzaei, S., Mohammadimehr, M. and Tounsi, A. (2019), "Nonlinear analysis of viscoelastic micro-composite beam with geometrical imperfection using FEM: MSGT electro-magneto-elastic bending, buckling and vibration solutions", *Struct. Eng. Mech., Int. J.*, **71**(5), 485-502. https://doi.org/10.12989/sem.2019.71.5.485.

Amanullah, M., AlArfaj, M.K. and Al-abdullatif, Z.A. (2011), "Preliminary test results of nano-based drilling fluids for oil and gas field application", *Proceedings of the SPE/IADC Drilling Conference and Exhibition: Society of Petroleum Engineers*, Amsterdam, Netherlands, January. https://doi.org/10.2118/139534-MS.

Ambartsumian, S.A. (1958), "On the theory of bending plates", *Izv. Otd. Tech. Nauk. An. SSSR.*, **5**(5), 69-77.

Amraei, J., Jam, J.E., Arab, B. and Firouz-Abadi, R.D. (2019), "Modeling the interphase region in carbon nanotube-reinforced polymer nanocomposites", *Polym. Compos.*, **40**(2), 1219-1234. https://doi.org/10.1002/pc.24950.

Arani, A.G., Maraghi, Z.K. and Arani, H.K. (2016), "Orthotropic patterns of Pasternak foundation in smart vibration analysis of magnetostrictive nanoplate", *Proc. Inst. Mech. Eng. Part C J. Mech. Eng. Sci.*, **230**(4), 559-572. https://doi.org/10.1177/0954406215579929.

Arefi, M., Bidgoli, E.M.R., Dimitri, R., Bacciocchi, M. and Tornabene, F. (2019), "Nonlocal bending analysis of curved nanobeams reinforced by graphene nanoplatelets", *Compos. Part B Eng.*, **166**, 1-12. https://doi.org/10.1016/j.compositesb.2018.11.092.

Asghar, S., Naeem, M.N., Hussain, M., Taj, M. and Tounsi, A. (2020), "Prediction and assessment of nonlocal natural frequencies of DWCNTs: Vibration analysis", *Comput. Concrete, Int. J.*, **25**(2), 133-144. https://doi.org/10.12989/cac.2020.25.2.133.

Asmatulu, R., Nguyen, P. and Asmatulu, E. (2013), *Nanotechnology Safety*, Elsevier, Burlington, USA. https://doi.org/10.1016/B978-0-444-59438-9.00005-9.

Aurojyoti, P., Raghu, P., Rajagopal, A. and Reddy, J.N. (2019), "An n-sided polygonal finite element for nonlocal nonlinear analysis of plates and laminates", *Int. J. Numer. Methods Eng.*, **120**(9), 1071-1107. https://doi.org/10.1002/nme.6171.

Balubaid, M., Tounsi, A., Dakhel, B. and Mahmoud, S.R. (2019), "Free vibration investigation of FG nanoscale plate using nonlocal two variables integral refined plate theory", *Comput. Concrete, Int. J.*, **24**(6), 579-586. https://doi.org/10.12989/cac.2019.24.6.579.

Bedia, W.A., Houari, M.S.A., Bessaim, A., Bousahla, A.A., Tounsi, A., Saeed, T. and Alhodaly, M.S. (2019), "A new hyperbolic two-unknown beam model for bending and buckling analysis of a nonlocal strain gradient nanobeams", *J. Nano Res.*, **57**, 175-191. https://doi.org/10.4028/www.scientific.net/JNanoR.57.175.

Bellal, M., Hebali, H., Heireche, H., Bousahla, A.A., Tounsi, A., Bourada, F., Mahmoud, S.R., Bedia, E.A.A. and Tounsi, A. (2020), "Buckling behavior of a single-layered graphene sheet resting on viscoelastic medium via nonlocal four-unknown integral model", *Steel Compos. Struct., Int. J.*, **34**(5), 643-655. https://doi.org/10.12989/scs.2020.34.5.643.

Berghouti, H., Adda Bedia, E.A., Benkhedda, A. and Tounsi, A. (2019), "Vibration analysis of nonlocal porous nanobeams made of functionally graded material", *Adv. Nano Res., Int. J.*, **7**(5),

351-364. https://doi.org/10.12989/anr.2019.7.5.351.

Bourada, F., Bousahla, A.A., Tounsi, A., Bedia, E.A., Mahmoud, S.R., Benrahou, K.H. and Tounsi, A. (2020), "Stability and dynamic analyses of SW-CNT reinforced concrete beam resting on elastic-foundation", *Comput. Concrete, Int. J.*, **25**(6), 485-495. https://doi.org/10.12989/cac.2020.25.6.485.

Bousahla, A.A., Bourada, F., Mahmoud, S.R., Tounsi, A., Algarni, A., Bedia, E.A. and Tounsi, A. (2020), "Buckling and dynamic behavior of the simply supported CNT-RC beams using an integral-first shear deformation theory", *Comput. Concrete, Int. J.*, **25**(2), 155-166. https://doi.org/10.12989/cac.2020.25.2.155.

Boutaleb, S., Benrahou, K.H., Bakora, A., Algarni, A., Bousahla, A.A., Tounsi, A., Tounsi, A. and Mahmoud, S.R. (2019), "Dynamic analysis of nanosize FG rectangular plates based on simple nonlocal quasi 3D HSDT", *Adv. Nano Res., Int. J.*, **7**(3), 191-208. https://doi.org/10.12989/anr.2019.7.3.191.

Chikr, S.C., Kaci, A., Bousahla, A.A., Bourada, F., Tounsi, A., Bedia, E.A., Mahmoud, S.R., Benrahou, K.H. and Tounsi, A. (2020), "A novel four-unknown integral model for buckling response of FG sandwich plates resting on elastic foundations under various boundary conditions using Galerkin's approach", *Geomech. Eng., Int. J.*, **21**(5), 471-487. https://doi.org/10.12989/gae.2020.21.5.471.

Demir, Ē., Civalek, Ö. and Akgöz, B. (2010), "Free vibration analysis of carbon nanotubes based on shear deformable beam theory by discrete singular convolution technique", *Math. Comput. Appl.*, **15**(1), 57-65. https://doi.org/10.3390/mca15010057.

Duc, N.D., Lee, J., Nguyen-Thoi, T. and Thang, P.T. (2017), "Static response and free vibration of functionally graded carbon nanotube-reinforced composite rectangular plates resting on Winkler–Pasternak elastic foundations", *Aerosp. Sci. Technol.*, **68**, 391-402. https://doi.org/10.1016/j.ast.2017.05.032.

Duc, N.D., Hadavinia, H., Quan, T.Q. and Khoa, N.D. (2019), "Free vibration and nonlinear dynamic response of imperfect nanocomposite FG-CNTRC double curved shallow shells in thermal environment", *Eur. J. Mech. A Solids*, **75**, 355-366. https://doi.org/10.1016/j.euromechsol.2019.01.024.

Ebrahimi, F. and Dabbagh, A. (2019), "Vibration analysis of multi-scale hybrid nanocomposite plates based on a Halpin-Tsai homogenization model", *Compos. Part B Eng.*, **173**, 106955. https://doi.org/10.1016/j.compositesb.2019.106955.

Elkhatib, E., Mahdy, A., Mahmoud, A. and Moharem, M. (2019), "Efficient removal of Cd (II) from contaminated water and soils using nanoparticles from nitrogen fertilizer industry waste", *J. Environ. Health Sci. Eng.*, **17**, 1153-1161. https://doi.org/10.1007/s40201-019-00429-z.

Eringen, A.C. (1983), "On differential equations of nonlocal elasticity and solutions of screw dislocation and surface waves", *J. Appl. Phys.*, **54**(9), 4703-4710. https://doi.org/10.1063/1.332803.

Esawi, A.M.K., Morsi, K., Sayed, A., Taher, M. and Lanka, S. (2010), "Effect of carbon nanotube (CNT) content on the mechanical properties of CNT-reinforced aluminium composites", *Compos. Sci. Technol.*, **70**(16), 2237-2241. https://doi.org/10.1016/j.compscitech.2010.05.004

Farajpour, A., Yazdi, M.H., Rastgoo, A., Loghmani, M. and Mohammadi, M. (2016), "Nonlocal nonlinear plate model for large amplitude vibration of magneto-electro-elastic nanoplates", *Compos. Struct.*, **140**, 323-336. https://doi.org/10.1016/j.compstruct.2015.12.039.

Gopalakrishnan, S. and Narendar, S. (2013), *Wave Propagation in Nanostructures: Nonlocal Continuum Mechanics Formulations*, Springer, New York, USA.

Grover, N., Maiti, D.K. and Singh, B.N. (2013), "A new inverse hyperbolic shear deformation theory for static and buckling analysis of laminated composite and sandwich plates", *Compos. Struct.*, **95**, 667-675. https://doi.org/10.1016/j.compstruct.2012.08.012.

Han, H., Hantschel, T., Strakos, L., Vystavel, T., Baryshnikova, M., Mols, Y., Kunert, B., Langer, R., Vandervorst, W. and Caymax, M. (2019), "Application of electron channeling contrast imaging to 3D semiconductor structures through proper detector configurations", *Ultramicroscopy*, **210**, 112928. https://doi.org/10.1016/j.ultramic.2019.112928.

Hanus, M.J. and Harris, A.T. (2013), "Nanotechnology innovations for the construction industry", *Prog. Mater. Sci.*, **58**(7), 1056-1102. https://doi.org/10.1016/j.pmatsci.2013.04.001.

Hosseini-Hashemi, S., Arpanahi, R.A., Rahmanian, S. and Ahmadi-Savadkoohi, A. (2019), "Free vibration analysis of nano-plate in viscous fluid medium using nonlocal elasticity", *Eur. J. Mech. A Solids*, **74**, 440-448. https://doi.org/10.1016/j.euromechsol.2019.01.002.

Hussain, M., Naeem, M.N., Tounsi, A. and Taj, M. (2019), "Nonlocal effect on the vibration of armchair and zigzag SWCNTs with bending rigidity", *Adv. Nano Res., Int. J.*, **7**(6), 431-442. https://doi.org/10.12989/anr.2019.7.6.431.

Ji, X., Li, X., Yu, H., Zhang, W. and Dong, H. (2019), "Study on the carbon nanotubes reinforced nanocomposite coatings", *Diam. Relat. Mater.*, **91**, 247-254. https://doi.org/10.1016/j.diamond.2018.11.027.

Kaczkowski, Z. (1968), *Plates-Statical Calculations*, Arkady, Warsaw, Poland.

Kaddari, M., Kaci, A., Bousahla, A.A., Tounsi, A., Bourada, F., Tounsi, A., Bedia, E.A. and Al-Osta, M.A. (2020), "A study on the structural behaviour of functionally graded porous plates on elastic foundation using a new quasi-3D model: Bending and free vibration analysis", *Comput. Concrete, Int. J.*, **25**(1), 37-57. https://doi.org/10.12989/cac.2020.25.1.037.

Karami, B. and Janghorban, M. (2019), "On the dynamics of porous nanotubes with variable material properties and variable thickness", *Int. J. Eng. Sci.*, **136**, 53-66. https://doi.org/10.1016/j.ijengsci.2019.01.002.

Karami, B., Janghorban, M. and Tounsi, A. (2019a), "Galerkin's approach for buckling analysis of functionally graded anisotropic nanoplates/different boundary conditions", *Eng. Comput.*, **35**(4), 1297-1316. https://doi.org/10.1007/s00366-018-0664-9.

Karami, B., Janghorban, M., Shahsavari, D., Dimitri, R. and Tornabene, F. (2019b), "Nonlocal buckling analysis of composite curved beams reinforced with functionally graded carbon nanotubes", *Molecules*, **24**(15), 2750. https://doi.org/10.3390/molecules24152750.

Karami, B., Shahsavari, D., Janghorban, M. and Li, L. (2019c), "Influence of homogenization schemes on vibration of functionally graded curved microbeams", *Compos. Struct.*, **216**, 67-79. https://doi.org/10.1016/j.compstruct.2019.02.089.

Karami, B., Shahsavari, D., Janghorban, M. and Li, L. (2019d), "On the resonance of functionally graded nanoplates using bi-Helmholtz nonlocal strain gradient theory", *Int. J. Eng. Sci.*, **144**, 103143. https://doi.org/10.1016/j.ijengsci.2019.103143.

Karami, B., Shahsavari, D., Li, L., Karami, M. and Janghorban, M. (2019e), "Thermal buckling of embedded sandwich piezoelectric nanoplates with functionally graded core by a nonlocal second-order shear deformation theory", *Proc. Inst. Mech. Eng. Part C J. Mech. Eng. Sci.*, **233**(1), 287-301. https://doi.org/10.1177/0954406218756451.

Khiloun, M., Bousahla, A.A., Kaci, A., Bessaim, A., Tounsi, A. and Mahmoud, S.R. (2020), "Analytical modeling of bending and vibration of thick advanced composite plates using a four-variable quasi 3D HSDT", *Eng. Comput.*, **36**(3), 807-821. https://doi.org/10.1007/s00366-019-00732-1.

Kim, M., Park, Y.B., Okoli, O.I. and Zhang, C. (2009), "Processing, characterization, and modeling of carbon nanotube-reinforced multiscale composites", *Compos. Sci. Technol.*, **69**(3-4), 335-342. https://doi.org/10.1016/j.compscitech.2008.10.019.

Kong, X. and Ohadi, M. (2010), "Applications of micro and nano technologies in the oil and gas industry-overview of the recent progress", *Proceedings of the International Petroleum Exhibition and Conference: Society of Petroleum Engineers*, Abu Dhabi, UAE, January. https://doi.org/10.2118/138241-MS.

Lei, Z.X., Liew, K.M. and Yu, J.L. (2013), "Buckling analysis of functionally graded carbon nanotube-reinforced composite plates using the element-free kp-Ritz method", *Compos. Struct.*, **98**, 160-168. https://doi.org/10.1016/j.compstruct.2012.11.006.

Li, Y.S. (2014), "Buckling analysis of magnetoelectroelastic plate resting on Pasternak elastic foundation", *Mech. Res. Commun.*, **56**, 104-114. https://doi.org/10.1016/j.mechrescom.2013.12.007.

Li, L. and Hu, Y. (2017), "Torsional vibration of bi-directional functionally graded nanotubes based on nonlocal elasticity theory", *Compos. Struct.*, **172**, 242-250. https://doi.org/10.1016/j.compstruct.2017.03.097.

Li, G.Y., Wang, P.M. and Zhao, X. (2007), "Pressure-sensitive properties and microstructure of carbon nanotube reinforced cement composites", *Cement Concrete Compos.*, **29**(5), 377-382. https://doi.org/10.1016/j.cemconcomp.2006.12.011.

Li, Z., Nambiar, S., Zheng, W. and Yeow, J.T.W. (2013), "PDMS/single-walled carbon nanotube composite for proton radiation shielding in space applications", *Mater. Lett.*, **108**, 79-83. https://doi.org/10.1016/j.matlet.2013.06.030.

Li, L., Hu, Y. and Ling, L. (2015), "Flexural wave propagation in small-scaled functionally graded beams via a nonlocal strain gradient theory", *Compos. Struct.*, **133**, 1079-1092. https://doi.org/10.1016/j.compstruct.2015.08.014.

Lu, L., Guo, X. and Zhao, J. (2017), "A unified nonlocal strain gradient model for nanobeams and the importance of higher order terms", *Int. J. Eng. Sci.*, **119**, 265-277. https://doi.org/10.1016/j.ijengsci.2017.06.024.

Mantari, J.L., Oktem, A.S. and Soares, C.G. (2011), "Static and dynamic analysis of laminated composite and sandwich plates and shells by using a new higher-order shear deformation theory", *Compos. Struct.*, **94**(1), 37-49. https://doi.org/10.1016/j.compstruct.2011.07.020.

Mantari, J.L., Oktem, A.S. and Soares, C.G. (2012), "A new higher order shear deformation theory for sandwich and composite laminated plates", *Compos. Part B Eng.*, **43**(3), 1489-1499. https://doi.org/10.1016/j.compositesb.2011.07.017.

Matouk, H., Bousahla, A.A., Heireche, H., Bourada, F., Bedia, E. A., Tounsi, A., Mahmoud, S.R., Tounsi, A. and Benrahou, K.H. (2020), "Investigation on hygro-thermal vibration of P-FG and symmetric S-FG nanobeam using integral Timoshenko beam theory", *Adv. Nano Res., Int. J.*, **8**(4), 293-305. https://doi.org/10.12989/anr.2020.8.4.293.

Megahed, A.A.E.W. and Megahed, M. (2017), "Fabrication and characterization of functionally graded nanoclay/glass fiber/epoxy hybrid nanocomposite laminates", *Iran. Polym. J.*, **26**(9), 673-680. https://doi.org/10.1007/s13726-017-0552-y.

Mirzavand, B. and Eslami, M.R. (2011), "A closed-form solution for thermal buckling of piezoelectric FGM rectangular plates with temperature-dependent properties", *Acta Mech.*, **218**(1-2), 87-101. https://doi.org/10.1007/s00707-010-0402-x.

Moghadam, A.D., Omrani, E., Menezes, P.L. and Rohatgi, P.K. (2015), "Mechanical and tribological properties of self-lubricating metal matrix nanocomposites reinforced by carbon nanotubes (CNTs) and graphene–a review", *Compos. Part B Eng.*, **77**, 402-420. https://doi.org/10.1016/j.compositesb.2015.03.014.

Nami, M.R. and Janghorban, M. (2014a), "Bending analysis of rectangular nanoplates based on two variable refined plate theory using strain gradient elasticity theory", *Proceedings of the 22nd Annual International Conference on Mechanical Engineering-ISME2014*, , Ahvaz, Iran, April.

Nami, M.R. and Janghorban, M. (2014b), "Resonance behavior of FG rectangular micro/nano plate based on nonlocal elasticity theory and strain gradient theory with one gradient constant", *Compos. Struct.*, **111**, 349-353. https://doi.org/10.1016/j.compstruct.2014.01.012.

Nami, M.R. and Janghorban, M. (2015a), "Dynamic analysis of isotropic nanoplates subjected to moving load using state-space method based on nonlocal second order plate theory", *J. Mech. Sci. Technol.*, **29**(6), 2423-2426. https://doi.org/10.1007/s12206-015-0539-6.

Nami, M.R. and Janghorban, M. (2015b), "Free vibration analysis of rectangular nanoplates based on two-variable refined plate theory using a new strain gradient elasticity theory", *J. Brazilian Soc. Mech. Sci. Eng.*, **37**(1), 313-324. https://doi.org/10.1007/s4043.

Nami, M.R., Janghorban, M. and Damadam, M. (2015), "Thermal buckling analysis of functionally graded rectangular nanoplates based on nonlocal third-order shear deformation theory", *Aerosp. Sci Technol.*, **41**, 7-15. https://doi.org/10.1016/j.ast.2014.12.001.

Nardi, T., Leterrier, Y., Karimi, A. and Månson, J.A.E. (2014), "A novel synthetic strategy for bioinspired functionally graded nanocomposites employing magnetic field gradients", *RSC Adv.*, **4**(14), 7246-7255. https://doi.org/10.1039/C3RA46731G.

Nardi, T., Hammerquist, C., Nairn, J.A., Karimi, A., Månson, J.A.E. and Leterrier, Y. (2015), "Nanoindentation of functionally graded polymer nanocomposites: Assessment of the strengthening parameters through experiments and modeling", *Front. Mater.*, **2**, 57. https://doi.org/10.3389/fmats.2015.00057.

Panc, V. (1975), *Theories of Elastic Plates*, Academia, Prague, Czech Republic.

Peddieson, J., Buchanan, G.R. and McNitt, R.P. (2003), "Application of nonlocal continuum models to nano-technology", *Int. J. Eng. Sci.*, **41**(3-5), 305-312. https://doi.org/10.1016/S0020-7225(02)00210-0.

Phung-Van, P., Abdel-Wahab, M., Liew, KM., Bordas, S.P.A. and Nguyen-Xuan, H. (2015), "Isogeometric analysis of functionally graded carbon nanotube-reinforced composite plates using higher-order shear deformation theory", *Compos. Struct.*, **123**, 137-149. https://doi.org/10.1016/j.compstruct.2014.12.021.

Pradhan, S.C. and Murmu, T. (2010), "Application of nonlocal elasticity and DQM in the flapwise bending vibration of a rotating nanocantilever", *Physica E Low Dimens. Syst. Nanostruct.*, **42**(7), 1944-1949. https://doi.org/10.1016/j.physe.2010.03.004.

Rabhi, M., Benrahou, K.H., Kaci, A., Houari, M.S.A., Bourada, F., Bousahla, A.A., Tounsi, A., Adda Bedia, A.A., Mahmoud, S.R. and Tounsi, A. (2020), "A new innovative 3-unknowns HSDT for buckling and free vibration of exponentially graded sandwich plates resting on elastic foundations under various boundary conditions", *Geomech. Eng., Int. J.*, **22**(2), 119-132. https://doi.org/10.12989/gae.2020.22.2.119.

Rad, A.B. (2018), "Static analysis of non-uniform 2D functionally graded auxetic-porous circular plates interacting with the gradient elastic foundations involving friction force", *Aerosp. Sci. Technol.*, **76**, 315-339. https://doi.org/10.1016/j.ast.2018.01.036.

Raghu, P., Preethi, K., Rajagopal, A. and Reddy, J.N. (2016), "Nonlocal third-order shear deformation theory for analysis of laminated plates considering surface stress effects", *Compos. Struct.*, **139**, 13-29.

https://doi.org/10.1016/j.compstruct.2015.11.068.

Rahmani, M.C., Kaci, A., Bousahla, A.A., Bourada, F., Tounsi, A., Bedia, E.A., Mahmoud, S.R., Benrahou, K.H. and Tounsi, A. (2020), "Influence of boundary conditions on the bending and free vibration behavior of FGM sandwich plates using a four-unknown refined integral plate theory", *Comput. Concrete, Int. J.*, **25**(3), 225-244. https://doi.org/10.12989/cac.2020.25.3.225.

Reddy, J.N. (1984), "A simple higher-order theory for laminated composite plates", *J. Appl. Mech.*, **51**(4), 745-752. https://doi.org/10.1115/1.3167719.

Reddy, J.N. (2007), "Nonlocal theories for bending, buckling and vibration of beams", *Int. J. Eng. Sci.*, **45**(2-8), 288-307. https://doi.org/10.1016/j.ijengsci.2007.04.004.

Refrafi, S., Bousahla, A.A., Bouhadra, A., Menasria, A., Bourada, F., Tounsi, A., Bedia, E.A.A., Mahmoud, S.R., Benrahou, K.H. and Tounsi, A. (2020), "Effects of hygro-thermo-mechanical conditions on the buckling of FG sandwich plates resting on elastic foundations", *Comput. Concrete, Int. J.*, **25**(4), 311-325. https://doi.org/10.12989/cac.2020.25.4.311.

Reissner, E. (1975), "On transverse bending of plates, including the effect of transverse shear deformation", *Int. J. Solids Struct.*, **11**(5), 569-573. https://doi.org/10.1016/0020-7683(75)90030-X.

Safaei, B., Moradi-Dastjerdi, R., Qin, Z. and Chu, F. (2019), "Frequency-dependent forced vibration analysis of nanocomposite sandwich plate under thermo-mechanical loads", *Compos. Part B Eng.*, **161**, 44-54. https://doi.org/10.1016/j.compositesb.2018.10.049.

Shariati, A., Ghabussi, A., Habibi, M., Safarpour, H., Safarpour, M., Tounsi, A. and Safa, M. (2020), "Extremely large oscillation and nonlinear frequency of a multi-scale hybrid disk resting on nonlinear elastic foundation", *Thin-Wall. Struct.*, **154**, 106840. https://doi.org/10.1016/j.tws.2020.106840.

She, G.L., Yuan, F.G., Karami, B., Ren, Y.R. and Xiao, W.S. (2019), "On nonlinear bending behavior of FG porous curved nanotubes", *Int. J. Eng. Sci.*, **135**, 58-74. https://doi.org/10.1016/j.ijengsci.2018.11.005.

Shen, H.S. (2009), "Nonlinear bending of functionally graded carbon nanotube-reinforced composite plates in thermal environments", *Compos. Struct.*, **91**(1), 9-19. https://doi.org/10.1016/j.compstruct.2009.04.026.

Shiva, K., Raghu, P., Rajagopal, A. and Reddy, J.N. (2019), "Nonlocal buckling analysis of laminated composite plates considering surface stress effects", *Compos. Struct.*, **226**, 111216. https://doi.org/10.1016/j.compstruct.2019.111216.

Shokrieh, M.M. and Moshrefzadeh-Sani, H. (2016), "On the constant parameters of Halpin-Tsai equation", *Polymer*, **106**, 14-20. https://doi.org/10.1016/j.polymer.2016.10.049.

Singh, D.B. and Singh, B.N. (2017), "New higher order shear deformation theories for free vibration and buckling analysis of laminated and braided composite plates", *Int. J. Mech. Sci.*, **131**, 265-277. https://doi.org/10.1016/j.ijmecsci.2017.06.053.

Srividhya, S., Basant, K., Gupta, R.K., Rajagopal, A. and Reddy, J.N. (2018a), "Influence of the homogenization scheme on the bending response of functionally graded plates", *Acta Mech.*, **229**(10), 4071-4089. https://doi.org/10.1007/s00707-018-2223-2.

Srividhya, S., Raghu, P., Rajagopal, A. and Reddy, J.N. (2018b), "Nonlocal nonlinear analysis of functionally graded plates using third-order shear deformation theory", *Int. J. Eng. Sci.*, **125**, 1-22. https://doi.org/10.1016/j.ijengsci.2017.12.006.

Taj, M., Majeed, A., Hussain, M., Naeem, M.N., Safeer, M., Ahmad, M., Khan, H.U. and Tounsi, A. (2020), "Non-local orthotropic elastic shell model for vibration analysis of protein microtubules", *Comput. Concrete, Int. J.*, **25**(3), 245-253. https://doi.org/10.12989/cac.2020.25.3.245.

Tounsi, A., Al-Dulaijan, S.U., Al-Osta, M.A., Chikh, A., Al-Zahrani, M.M., Sharif, A. and Tounsi, A. (2020), "A four variable trigonometric integral plate theory for hygro-thermo-mechanical bending analysis of AFG ceramic-metal plates resting on a two-parameter elastic foundation", *Steel Compos. Struct., Int. J.*, **34**(4), 511-524. https://doi.org/10.12989/scs.2020.34.4.511.

Touratier, M. (1991), "An efficient standard plate theory", *Int. J. Eng. Sci.*, **29**(8), 901-916. https://doi.org/10.1016/0020-7225(91)90165-Y.

Vellingiri, K., Ramachandran, T. and Senthilkumar, M. (2013), "Eco-friendly application of nano chitosan in antimicrobial coatings in the textile industry", *Nanosci. Nanotechnol. Lett.*, **5**(5), 519-529. https://doi.org/10.1166/nnl.2013.1575.

Wang, Y.Z. and Li, F.M. (2012), "Static bending behaviors of nanoplate embedded in elastic matrix with small scale effects", *Mech. Res. Commun.*, **41**, 44-48. https://doi.org/10.1016/j.mechrescom.2012.02.008.

Wu, Q., Chen, H. and Gao, W. (2019), "Nonlocal strain gradient forced vibrations of FG-GPLRC nanocomposite microbeams", *Eng. Comput.*, **36**, 1739-1750. https://doi.org/10.1007/s00366-019-00794-1.

Zhang, Q., Huang, J.Q., Qian, W.Z., Zhang, Y.Y. and Wei, F. (2013), "The road for nanomaterials industry: A review of carbon nanotube production, post-treatment and bulk applications for composites and energy storage", *Small*, **9**(8), 1237-1265. https://doi.org/10.1002/smll.201203252.

Zhu, J., Peng, H., Rodriguez-Macias, F., Margrave, J.L., Khabashesku, V.N., Imam, A.M., Lozano, K. and Barrera, E.V. (2004), "Reinforcing epoxy polymer composites through covalent integration of functionalized nanotubes", *Adv. Funct. Mater.*, **14**(7), 643-648. https://doi.org/10.1002/adfm.200305162.

Zhu, P., Lei, Z.X. and Liew, K.M. (2012a), "Static and free vibration analyses of carbon nanotube-reinforced composite plates using finite element method with first order shear deformation plate theory", *Compos. Struct.*, **94**(4), 1450-1460. https://doi.org/10.1016/j.compstruct.2011.11.010.

Zhu, Z., Garcia-Gancedo, L., Flewitt, A.J., Xie, H., Moussy, F. and Milne, W.I. (2012b), "A critical review of glucose biosensors based on carbon nanomaterials: Carbon nanotubes and graphene", *Sensors*, **12**(5), 5996-6022. https://doi.org/10.3390/s120505996

AT

Appendix

Here, a closed form solution for buckling analysis of FG-CNTRC is presented.

N0 = (-a1*g1*k(3,3)*s1*y1 + a1*g1*k(3,3)*x1*t1 + a1*g1*n1*r1*y1 - a1*g1*n1*w1*t1
- a1*g1*o1*r1*x1 + a1*g1*o1*s1*w1 + a1*h1*l1*s1*y1 - a1*h1*l1*x1*t1 - a1*h1*n1*q1*y1
+ a1*h1*n1*u1*t1 + a1*h1*o1*q1*x1 - a1*h1*o1*u1*s1 - a1*i1*l1*r1*y1 + a1*i1*l1*w1*t1
+ a1*i1*k(3,3)*q1*y1 - a1*i1*k(3,3)*u1*t1 - a1*i1*o1*q1*w1 + a1*i1*o1*u1*r1 + a1*j1*l1*r1*x1
- a1*j1*l1*w1*s1 - a1*j1*k(3,3)*q1*x1 + a1*j1*k(3,3)*u1*s1 + a1*j1*n1*q1*w1 - a1*j1*n1*u1*r1
+ b1*f1*k(3,3)*s1*y1 - b1*f1*k(3,3)*x1*t1 - b1*f1*n1*r1*y1 + b1*f1*n1*w1*t1 + b1*f1*o1*r1*x1
- b1*f1*o1*w1*s1 - b1*h1*k1*s1*y1 + b1*h1*k1*x1*t1 + b1*h1*n1*p1*y1 - b1*h1*n1*v1*t1
- b1*h1*o1*p1*x1 + b1*h1*o1*s1*v1 + b1*i1*k1*r1*y1 - b1*i1*k1*w1*t1 - b1*i1*k(3,3)*p1*y1
+ b1*i1*k(3,3)*v1*t1 + b1*i1*o1*p1*w1 - b1*i1*o1*v1*r1 - b1*j1*k1*r1*x1 + b1*j1*k1*w1*s1
+ b1*j1*k(3,3)*p1*x1 - b1*j1*k(3,3)*s1*v1 - b1*j1*n1*p1*w1 + b1*j1*n1*v1*r1 - c1*f1*l1*s1*y1
+ c1*f1*l1*x1*t1 + c1*f1*n1*q1*y1 - c1*f1*n1*u1*t1 - c1*f1*o1*q1*x1 + c1*f1*o1*s1*u1
+ c1*g1*k1*s1*y1 - c1*g1*k1*x1*t1 - c1*g1*n1*p1*y1 + c1*g1*n1*v1*t1 + c1*g1*o1*p1*x1
- c1*g1*o1*v1*s1 - c1*i1*k1*q1*y1 + c1*i1*k1*u1*t1 + c1*i1*l1*p1*y1 - c1*i1*l1*v1*t1
- c1*i1*o1*p1*u1 + c1*i1*o1*v1*q1 + c1*j1*k1*q1*x1 - c1*j1*k1*u1*s1 - c1*j1*l1*p1*x1
+ c1*j1*l1*v1*s1 + c1*j1*n1*p1*u1 - c1*j1*n1*v1*q1 + d1*f1*l1*r1*v1 - d1*f1*l1*w1*t1
- d1*f1*k(3,3)*q1*y1 + d1*f1*k(3,3)*u1*t1 + d1*f1*o1*q1*w1 - d1*f1*o1*u1*r1 - d1*g1*k1*r1*y1
+ d1*g1*k1*w1*t1 + d1*g1*k(3,3)*p1*y1 - d1*g1*k(3,3)*v1*t1 - d1*g1*o1*p1*w1 + d1*g1*o1*v1*r1
+ d1*h1*k1*q1*y1 - d1*h1*k1*u1*t1 - d1*h1*l1*p1*y1 + d1*h1*l1*v1*t1 + d1*h1*o1*p1*u1
- d1*h1*o1*v1*q1 - d1*j1*k1*q1*w1 + d1*j1*k1*u1*r1 + d1*j1*l1*p1*w1 - d1*j1*l1*v1*r1
- d1*j1*k(3,3)*p1*u1 + d1*j1*k(3,3)*v1*q1 - e1*f1*l1*r1*x1 + e1*f1*l1*w1*s1 + e1*f1*k(3,3)*q1*x1
- e1*f1*k(3,3)*u1*s1 - e1*f1*n1*q1*w1 + e1*f1*n1*u1*r1 + e1*g1*k1*r1*x1 - e1*g1*k1*w1*s1
- e1*g1*k(3,3)*p1*x1 + e1*g1*k(3,3)*v1*s1 + e1*g1*n1*p1*w1 - e1*g1*n1*v1*r1 - e1*h1*k1*q1*x1
+ e1*h1*k1*u1*s1 + e1*h1*l1*p1*x1 - e1*h1*l1*v1*s1 - e1*h1*n1*p1*u1 + e1*h1*n1*v1*q1
+ e1*i1*k1*q1*w1 - e1*i1*k1*u1*r1 - e1*i1*l1*p1*w1 + e1*i1*l1*v1*r1 + e1*i1*k(3,3)*p1*u1
- e1*i1*k(3,3)*v1*q1)/($N(3,3)$ ∗ (a1*g1*s1*y1 - a1*g1*x1*t1 - a1*i1*q1*y1 + a1*i1*u1*t1
+ a1*j1*q1*x1 - a1*j1*u1*s1 - b1*f1*s1*y1 + b1*f1*x1*t1 + b1*i1*p1*y1 - b1*i1*v1*t1 - b1*j1*p1*x1
+ b1*j1*s1*v1 + d1*f1*q1*y1 - d1*f1*u1*t1 - d1*g1*p1*y1 + d1*g1*v1*t1 + d1*j1*p1*u1 - d1*j1*v1*q1
- e1*f1*q1*x1 + e1*f1*u1*s1 + e1*g1*p1*x1 - e1*g1*v1*s1 - e1*i1*p1*u1 + e1*i1*v1*q1))

where

a1 = k(1,1); b1 = k(1,2); c1 = k(1,3); d1 = k(1,4); e1 = k(1,5); f1 = k(2,1); g1 = k(2,2); h1 = k(2,3); i1 = k(2,4); j1 = k(2,5); k1 = k(3,1); l1 = k(3,2); n1 = k(3,4); o1 = k(3,5); p1 = k(4,1); q1 = k(4,2); r1 = k(4,3); s1 = k(4,4); t1 = k(4,5); v1 = k(5,1); u1 = k(5,2); w1 = k(5,3); x1 = k(5,4); y1 = k(5,5)